Analysis of range-scale topographic changes from digital topography in the southern-central Andes (latitudes 32° to 39°S)

Jennifer J. McIntosh
Department of Earth Sciences
Dalhousie University

Advisor
John Gosse
Department of Earth Sciences
Dalhousie University

Submitted in partial fulfillment of the requirements for the
Degree of Honours Bachelor of Science Earth Science
Dalhousie University, Halifax, Nova Scotia

May 2004

DALHOUSIE
University

Department of Earth Sciences
Life Sciences Centre, Room 3006
Halifax, Nova Scotia
B3H 4J1
Tel: (902) 494-2358
Fax: (902) 494-6889
E-mail: earth.sciences@dal.ca
WWW: http://meguma.earthsciences.dal.ca

Date: April 30, 2004

Author: Jennifer McIntosh
Title: Analysis of range-scale topographic changes from digital topography in the southern-central Andes (latitudes 32° to 39°S)

Degree: B. Sc.
Convocation: May 25, 2004

Abstract

There is currently insufficient information regarding topographic changes in the southern Andes from 32° to 39°S. The Andes between 32° and 39° are separated into three zones with distinct elevations: 32°-35°, 35°-36° and 36°-39°. In the northern zone, peak elevation is 6000m, peak elevation gradually decreases from 35° to 36° and south of 39° peaks elevation is 2600m. The goal of this analysis is to determine whether other geomorphic indices such as relief, stream concavity, hypsometry, tributary asymmetry and mountain front sinuosity would also distinguish these zones. A digital elevation map (DEM) acquired from the Shuttle Radar Topography Mission is analyzed using RiverTools- a software package for river network and topography analysis, and ArcMap. In a geomorphometric analysis of any kind, it is important to measure a variety of parameters to establish trends in uplift, erosion and mountain front stability. From north to south, basin relief is decreasiing and hypsometric integral and slope are both decreasing. Mountain front sinuosity increases moving south, indicating more rounded and mature mountains. Tributary asymmetry suggests differential uplift patterns in the study area, with uplift occurring in the north and in the south-east. Stream concavity shows no conclusive pattern. Using these metrics, it was possible to distinguish the zones of high tectonic activity in the area- the Liquine-Ofqui fault and the Aconcagua fold and thrust zone. Tests of mountain front sinuosity of the range and hypsometry of the basins showed that the southern mountains are more glaciated than other regions. Uplift determined by tributary asymmetry and mountain front sinuosity in the area surrounding the longitudinal valley between 32° and 34°S helped confirm that present-day uplift of the valley has taken place since the Late-Miocene. Based on these measurements of the topography, zones of quantifiably different topography do not exist however the geomorphometrics successfully identified many structural and surficial features of the study area.

Table of Contents

List of figures and tables

Acknowledgements

I would like to thank John Gosse for his support in writing this thesis. Without his knowledge, encouragement and humour, this paper would not have been such a pleasure to write. I would also like to thank Dorothy Godfrey-Smith and Marcos Zentilli for providing feedback in the final stages of this thesis. I would like to thank Guang Yang for helping me acquire software and upgrade packages. Finally, I would like to thank Lawrence Plug, Jane Staiger, Sophie Baker, Jose Antinao and Andrew Hilchey for their advice and encouragement.

Chapter 1.

Range-scale topographic changes in the southern central Andes

1.1 Introduction

The topography of an area reflects the interactions of all surface and tectonic processes. Sub-range scale landforms, such as streams and basins, record a few processes working over short time scales and limited spatial scales. Range-scale landscapes, such as a volcanic arc, are more a function of longer term processes. This thesis sets out to describe the late Cenozoic landscape evolution of the topography between latitudes 32° and 39° S in the Andes by analyzing range-scale features such as major river channels, drainage basins, and relief.

The measurement of landscape shape allows geomorphologists to objectively compare similar landforms and contrast the levels of influence of tectonic activity and surface processes (Keller and Pinter 1998). Topographic analyses of the Taiwan mountains ranges (Willemen and Knuepfer 1994) and the Himalayas (Burbank 2003) have yielded much information about tectonic and surficial processes. Landscape evolution and other analysis in other parts of the world has also lead to relationships between these processes, for example in the Rocky Mountains of New Mexico (Frankel and Pazzaglia unpub), New Zealand (Porter 1975), and extensively throughout the Andes (Ramos et al. 1996, Markgraf 1987, Jordan et al. 1983, Giambiagi and Ramos 2003, Montgomery et al. 2002, Allmendinger et al. 1983 and Allmendinger et al. 1990). These

kinds of studies are useful in developing numerical models by providing parameters of real landscapes and topography (Kooi and Beaumont 1994, Liu and Bird 2002).

Considerable effort to understand the nature of the topography of the Andes has focussed on the effects of tectonic and climate processes. The complex geometry of the subduction of the Nazca plate (change in subduction angle, spatial transition of subduction angle, style of angle change) may have first order control on the topography of the Andes, providing measurable zones of transitional topography where the geometry of the slab changes. Changes in slab dip are known to control changes in large scale topographic features (Giambiagi and Ramos 2003, Allmendinger et al. 1990 and 1983), and numerous papers address the tectonics of ranges of the southern Andes.

The effect of slab dip on the type of deformation (thin- or thick-skinned folding and thrusting) has been studied in several parts of the southern Andes (Ramos et al. 1996, Jordan et al. 1983). Kennan (2000) argues that the large scale geomorphology of the Andes reflects crustal thickening resulting mostly from crustal shortening, whereas erosion plays an important role in creating smaller scale (10 to 100km wavelength) topographic features. At 30° latitude, the shortening of the Precordillera accounts for 60 to 75% of the total shortening during the past 15 Ma, but accounts for less that 10% of the total convergence rate for this period (Allmendinger et al. 1990).

Several authors have found correlations between climate change and Andean uplift over the past 20 Ma. Sedimentological and paleoaltitudinal data have shown that the rain shadow effect generated by Andean uplift which reinforced the pre-existing climate regime was probably in place 15 Ma ago.

The effect of climate on several aspects of the Andes is well documented. Changes in elevation, relief, and erosion over the entire Andes have been attributed to changes in climate, most notably a decrease in elevation at 35°S when the high Andes intersect the perennial snow line (Montgomery et al. 2001, Porter 1975, Abele 1989). Latitudinal changes in erosion and denudation correspond to diverse climatic zones determined by convectional precipitation, aridity, vegetation and wind patterns, as well as uplift and volcanism (Abele, 1989). Changes in the paleoclimate of the Andes reflected in palynological information have been recorded for the most recent glacial times (Markgraf 1987). High mountain ranges in the central Andes may be controlled by climates which inhibit or promote sedimentation and focus plate-driving forces, which in turn raises shear stresses to levels high enough to support >3000 m elevations (Lamb and Davis, 2003).

Relationships between climate and topography have been documented in the Taiwan mountain ranges. Spatial and temporal variations in uplift rate and pattern along the Taiwan orogen were inferred from the classification of 32 different geomorphometric indices including stream profiles, drainage basin perimeters, traces of the mountain-piedmont junction, elevation of the range crest and many others (Willemin and Knuepfer 1994). Their results included broad patterns in small scale topography by the comparison of drainage basin perimeters, stream channels and the mountain front sinuosity.

The character of the landscape revealed distinct geomorphic domains with variations in uplift of the mountain front with respect to the valley floor. The authors used geomorphic features to determine aspects of the kinematic evolution of the Central Range, and this was the first study to use this approach. This paper uses several of these

indices to analyze the topography: relief, basin relief, longitudinal profiles of streams, concavity of stream profiles, tributary asymmetry, hypsometry, and drainage area-slope information.

Topographic analysis and landscape evolution in the past have largely focussed on other parts of South America, particularly the central zone (Hartley 2003, Abele 1989, and Kennan 2000). It is important both to the work of my supervisor and to the work of others to determine the nature and the evolution of present day topography in order to understand the relationships between surficial and tectonic processes in this area, and apply this information to other parts of the world. Researchers now have access to high resolution digital elevation maps for all areas of the world through the Shuttle Radar Topography Mission (http://seamless.usgs.gov/, January 6, 2003), and a vast number of topographic analysis software to study them. These developments provide many ways to analyze small and large scale features of the earth in order to compliment the results of field work, thermochronology, exposure dating, and stratigraphy.

1.2 Hypothesis

The area of focus in this study is from latitudes 32° to 39°S and from 68° to 73° W (Figure 1.1). This region is a poorly-understood transition zone characterized by changing peak heights and relief decreasing to the south. Using software to analyze digital topography in this zone, the changes in elevation are assigned to three zones- high elevation (>5000 m peaks), intermediate elevations (from 3000 m to 5000m peaks) and low elevation (<3000 m peaks). This thesis will determine if there are topographic characteristics other than peak heights which follow this spatial zonation on the basis of

morphology and landscape history interpreted from DEM-based topographic analysis. It will also be possible to interpret unique features such as antecedent streams in light of the tectonic and surficial processes acting in this zone. The goal is to determine if latitudinal zones, such as the zones defined by relief, can be documented by changes in topographical characteristics such as relief, concavity of longitudinal profiles, hypsometric integral and slope of the inflection point of the hypsometric curve of drainage basins, differences in drainage area and slope of basins, tributary asymmetry and mountain front sinuosity.

From 32° to 34°S, mean elevation is 3800 m and mean relief is 430.7 ± 108 m. From 34° to 36°S, mean elevations drop from 3800 to 1800 m, and mean relief changes to 189.2 ± 76 m. Mountain front sinuosity shows an increasing trend to the south on both sides of the drainage divide. Hypsometric curves have decreasing integrals and slopes at the inflection point moving south. Analysis of tributary asymmetry reveals differential uplift and erosion patterns in two of these zones. Concavity reveals no clear pattern in the study area.

These results prove that analyses of range-scale features on digital elevation maps can be used to describe changes in landscape morphology caused by tectonic activity and surficial processes. This type of study can be used in collaboration with field work to determine quantitative rates of geomorphic processes, and can also stand alone as a preliminary analysis of range-scale topography. The transition zone in this study corresponds roughly to the transition in climate (Montgomery et al. 2001, Hartley 2003, Abele 1989, Lamb and Davis 2003, and Kennan 1999), and changes in subduction slab geometry (Ramos et al. 1996, Jordan et al. 1983, Allmendinger et al. 1990 and 1983).

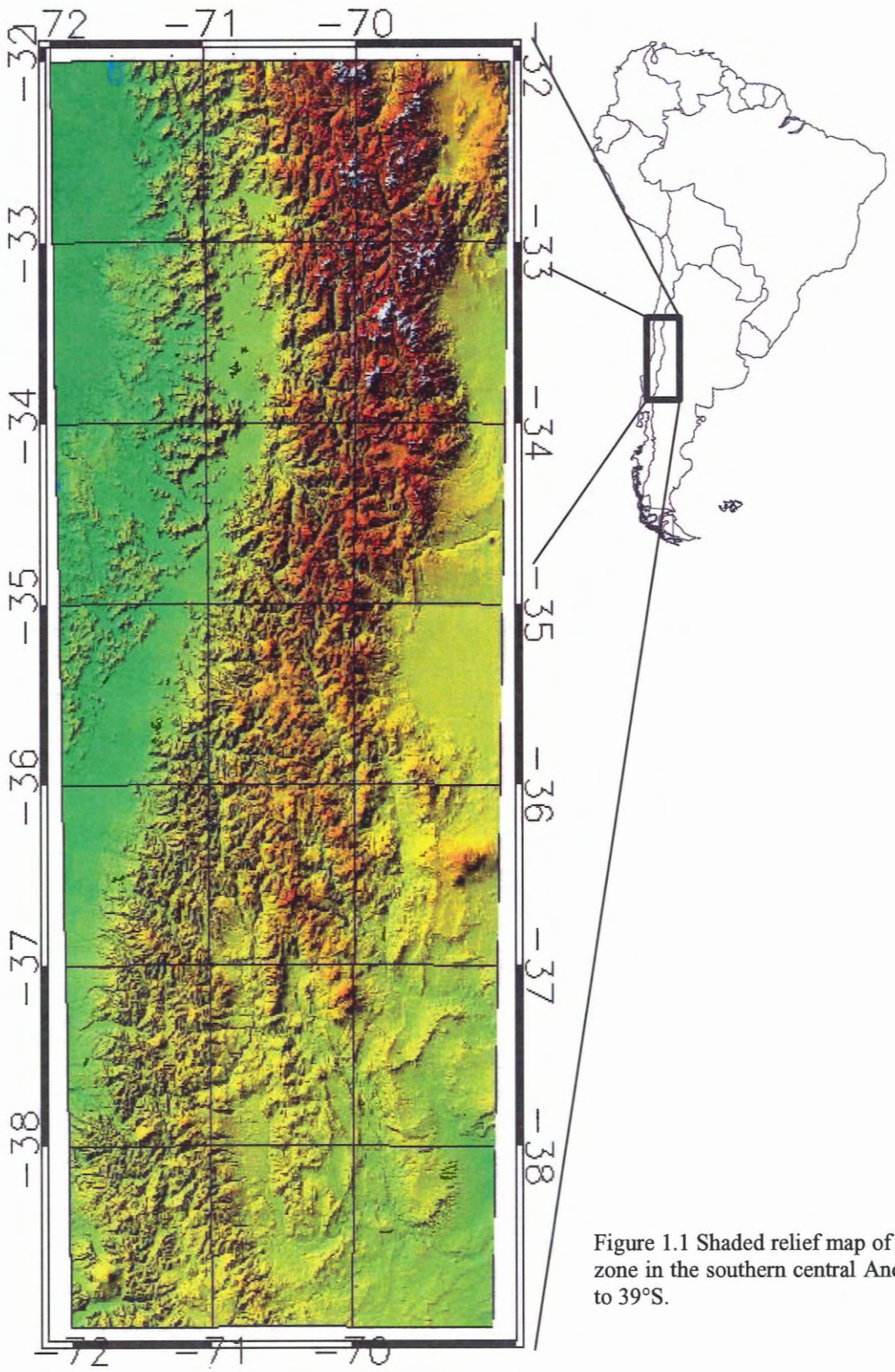

Figure 1.1 Shaded relief map of the transition zone in the southern central Andes, from 32° to 39°S.

Chapter 2.

Andean landscape evolution

2.1 Published conceptual models and related research

It is possible for the topography of a region to give sufficient clues about the evolution of the landscape in order to create a general understanding of how the topography came to be as we see it today. The Andes hold many clues about their past in their surficial geology and structures, and have been extensively studied from many aspects. The Andes extend along the length of western South America, and are far from uniform in elevation, width, distribution of ranges, and lithology. The northern Andes (5°N to 15°S) are a relatively narrow range of mountains and volcanoes. The central Andes (15° to 30°S) include the internally drained Altiplano and Puna regions, and are the widest region of the Andes. South of 30°S, the Andes become narrow and the ranges merge into a Principal Cordillera and a Coastal Cordillera, separated by a coastal

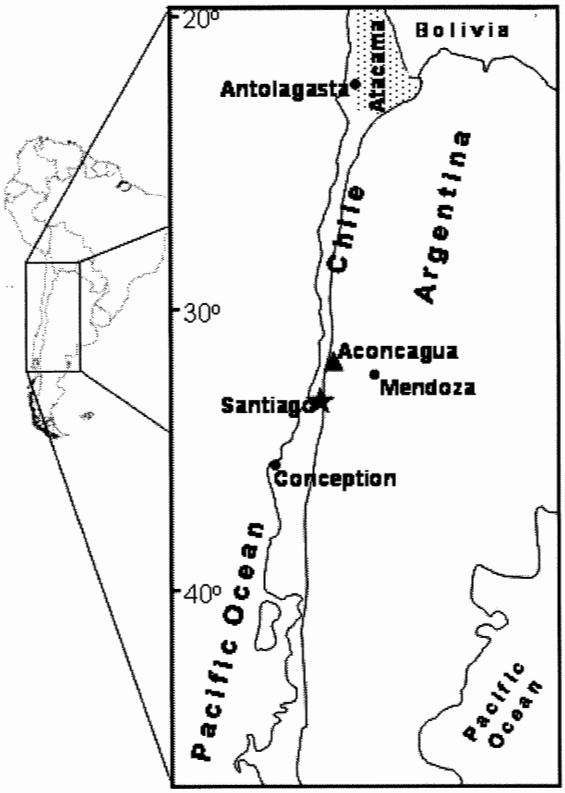

Figure 2.1 South America and the Central and Southern Andes. Political boundaries of Chile, Argentina and Bolivia are outlined, and the capital city of Chile is highlighted in the centre of the figure.

valley. In the southern Andes, glaciers exist in valleys but these decrease in abundance further south and ice caps dominate the topography. The most important processes to consider in the Andes are subduction of the Nazca Plate to the west, and differential precipitation and erosion along the range. These processes are the focus of much research to better understand the nature of the Andes and the cause and effect of processes and landforms. Between 32°S and 39°S, the Andes give several clues which have helped to determine the evolution of its topography. The north of this region is characterized by high elevations from 4000 m to 7000 m (average 4800 m), and the Aconcagua and Tupungatito mountains (Figure 2.1). The width of the Andean range changes from 600 km to 50 km is a relatively short distance. Accompanying this change in width is a change in the number of actual mountain ranges- from three to one around 30°S.

There are different ways to interpret landscape evolution- the two schools of thought regarding the formation of topographic features are that features are created mainly by tectonic processes, or surficial processes such as erosion. Slab dip geometry changes from steep to shallow subduction around 30-33°S, and many speculate this to have first order control over the topography of the region. Climate and erosion also play an important role in shaping the landscape, and must be considered in combination with tectonic forces.

Kennan (2000) describes the Andes as a "natural laboratory for the study of numerous processes which form an ocean-continent convergent margin". Changes in the dip of the subducting plate, elastic thickness of the continental plate, and the presence of thick sequences of Paleozoic sediments correlate with changes in the width of the plateau,

foreland shortening, and thick-skinned basement uplifts (Kennan 2000). Large-scale Andean geomorphology is likely intimately linked to crustal thickening processes such as magmatic accretion and horizontal shortening, but the chain of cause and effect between tectonic and surface processes and large-scale features is poorly known. There is no quantitative fission track or paleobotanical data from which to extract altitude or denudation rates from 25° to 35°S (Kennan 2000). Kennan (2000) notes that relief has not been in equilibrium since the late Pliocene; mean relief has oscillated throughout this time. Enhanced erosion and sedimentation rates are observed since 8.5 Ma, and rapid shortening to 400 m.

The Altiplano-Puna region in the central Andes is an internally drained system of basins from 15° to 25°S. Mean elevation in this plateau is ~4000 m, with peaks of up to 7000 m. The east-west watershed boundaries of the Altiplano-Puna have been constant for 25 Ma (Kennan 2000). Mean elevation and orogen width decrease to the north and south of these latitudes. In the north, elevations change to 500-1000 m with some peaks reaching 3000 m and south of 35° average elevations are ~3000 m (Kennan 2000). The tectonics in this area changes from shallow (0-10°) to moderate (~30°) dip but these are not separated by sharp tears, and may be caused by buoyancy changes in relatively younger crust (Kennan 2000). Shallow slabs have little to no asthenospheric wedge, and steep slabs are characterized by volcanic activity and an asthenospheric wedge (Kennan 2000).

Abele et al. (1989) described the geometry of the subducting Nazca plate in low angle dip zones (2°-15°S and 27°-33°S) and 30° dip zones (15°-24°S and >33°S). Abrupt changes in slab dip may indicate that resorption is dependent upon the angle of

subduction and the time involved (Abele et al. 1983). Above zones of high dip, deformation is thin-skinned and a major valley separates coastal mountains from the Principal Range. Above sub-horizontal slabs, there is no longitudinal valley and deformation is thin-skinned with basement crustal shortening (Abele et al. 1983). There is some disagreement between Abele et al. and Kennan and others as to the geometry of transitions between steep and sub-horizontal subduction angles. Kennan believes the transitions are zones of contortion (Kennan 2000), while Abele et al. (and others) interprets them as tears between the segments (Abele et al. 1983).

The geometry subducting slab at 33° such as the width of the transition from low angle to high angle subduction and the style of this transition, is not completely understood. There is also a pronounced change in geology at 34°30'S which coincides with the northern limit of the Mesozoic Neuquen basin. Late Paleozoic-early Mesozoic mountain building may also have created a prominent NW trending structural grain which intersects the Andes at 34°30'S (Abele et al. 1983).

Montgomery et al. (2001) believe that climatic zonations and the resulting differences in geomorphology processes are of first order importance in the morphology of mountain ranges. They defined four major zones- intertropical convergence zone (10°N to 3°S), subequatorial northern Andes (3° to 15°S), the subtropical belt of deserts (15° to 33°) and the southern Andes (>33°)- on the basis of hypsometry, cross-range asymmetry and maximum elevation of a mountain range. These zones are not dependent of orogenic effects but are features of the general circulation of the southern hemisphere and therefore may be considered a priori conditions under which the mountain range developed (Montgomery et al. 2001). The authors created an erosional index which

describes the net large scale erosional potential of a landscape, calculated by I_E = [sum P_iA_i]·S where I_E is the erosional intensity, P is the annual precipitation over the matrix of upslope grid cells, and A is the drainage area. Areas of maximum erosion were in the east of the northern Andes, in the west of the southern Andes, and in small, localized areas in the central Andes. Cross-range asymmetry is calculated by the fraction of the range volume draining west of the continental divide relative to the total range volume in a latitudinal band. It tracks latitudinal variations in moisture delivery due to prevailing wind direction. Their results showed that north of 2°S and south of 42°S, most the range lies of the west of the divide, and between 2° and 42° most of the range lies to the east. Hypsometric curved showed regionally consistent shapes in the north, central and southern Andes. The curves show fluvial, tectonic and glacial processes are the dominant processes in these zones (Montgomery et al. 2001). These correlations are consistent with actual variations in erosional processes, and describe how the nature of dominant erosion mechanism and rate relative to uplift are fundamental to topographic expression. Finally, examination of the perennial snow line reveals it roughly corresponds to the maximum elevations north of the 35° in the Andes (Satoh). The authors concluded that rates of erosion in glacial and periglacial environments (south of 35°S) are limiting factors on the relief of a mountain range (Montgomery et al. 2001).

The indices of erosion, cross-range asymmetry, and hypsometry show patterns linking climate zones and large scale-morphology which agree with the changing erosion and denudation rates suggested by Kennan (2000), but disagree with first order control on morphology. The correspondence of perennial snow line with peak height is similar to the idea put forth by Porter (1975) regarding equilibrium line altitudes. Equilibrium line

altitude, a parameter which marks the points of a glacier where the net mass is balanced, is sensitive to climate change and is an important indication of fluctuations in climate and hence erosion rates (Porter 1975). The southernmost Andes are highly glaciated however ELA analyses are not known to have been completed on the southern or central Andes. Analysis of ELA in other mountain ranges such as the Himalayas (Brozovic et al. 1997), New Zealand (Kirkbride and Matthews 1997), and the western United States (Brocklehurst et al. 2002) has yielded much information that could be applied throughout the Andes. Changes in ELA significantly increase or decrease the percent surface area covered by the glaciers at elevations close to the ELA (Brozovic et al. 1997). Any surface uplift results in a lowering of the ELA and an increase in the area covered by the glacier, which causes increased erosion in an attempt to bring the ELA back to its original position (Brozovic et al. 1997). Unique circumstances in relatively small basins can have a major impact on the hypsometry of a basin (Brocklehurst and Whipple 2002).

Lamb and Davis (2003) discuss correlations between shortening and uplift not addressed by Ramos et al. Given the shear stresses and the relevant subduction parameters calculated by Lamb and Davis (2003), the thermal structure of the Andes does not significantly change with latitude because "shear heating in the high shear stress segments more-or-less compensates for the lower heat flux from older oceanic lithosphere" (Lamb and Davis 2003). Plate interface shear stress dynamics are related to latitudinal changes in the coefficient of friction, or of pore fluid pressure or viscosity yield strength in the viscous/plastic zone caused by lithological changes at a scale of ~1000km caused by the presence or absence of trench sediment fill (Lamb and Davis 2003). The authors identify the range from 10°-33°30'S as starved of sediment fill and

hence exhibit higher shear stresses, and suggest these conditions persisted as far back as the Pliocene. Sediment starvation in this region is the result of the arid climate where there is virtually no runoff (Lamb and Davis 2003).

The relationship between an arid climate and lack of runoff which causes sediment starvation and hence affects plate interface shear stress dynamics is not addressed by other authors and is the link between dominant climate processes and dominant tectonic influences on range-scale topography.

Ramos et al. (1996) have demonstrated the conspicuous change along strike from thin-skinned to thick-skinned style fold and thrust belts. The amount of orogenic shortening in La Ramada is about 150km in the Principal Cordillera, and 40km of shortening occurs in the Precordillera, in the Aconcagua, shortening is 130km, and in the Malargue shortening has been calculated at 90km.

The position of the equilibrium line altitude with respect to the elevation of the cirque headwall and the basin outlet is an important variable in the hypsometry of the basin (Brocklehurst and Whipple 2002). Hypsometries and hypsometric curves are an indication of the relative degree of erosion and tectonic movements in neighbouring basins (Brocklehurst and Whipple 2002, Brozovic et al. 1997 and Riquelme 2002). Arthur Strahler analyzed basins and hypspometric curves in 1952 and found many applications of hypsometry to landscape evolution and topographic change. He found that the shape of a hypsometric curve could classify a basin as inequilibrium (youthful) and equilibrium (mature) (Strahler 1952). Mature basins with low relief, gentle slopes and low drainage density produce relatively high hypsometric integrals, while basins with high relief, steep slopes and stream gradients produce low hypsometric integrals (Strahler

1952). It is important to note however that curves with unique structures or processes may have more complicated curves whose integrals fall into a category which does not represent them (Strahler 1952).

The majority of literature on the range-scale morphology of the Central Andes points to tectonics as the primary control on the landscape. For example, the distribution of large morphostructural units of the Central Andes is controlled by the first-order segmentation of the Nazca plate at the Benioff-Wadaati zone (Ramos et al. 1996). The lack of a volcanic arc and the development of Precordillera and basement block uplifts are consequences of the shallowing of the subduction zone during post-Miocene times. Several morphostructural changes are not correlative with the Benioff zone geometry, such as the change from thin- to thick-skinned thrusting in the Principal Cordillera (Ramos et al. 1996). That Ramos et al. do not relate style of deformation to subduction geometry lends some credibility to other processes such as climate and erosion, but only indirectly. For instance, the trend of less contraction southward corresponds with many gradual surficial process changes mentioned by Montgomery et al (2001).

2.2 Testing the Hypothesis

In this analysis of range-scale topography, the scope ranges from 32° and 39°S in the Andes, encompassing changes in structures as well as geology (Abele 1989, Jordan et al. 1983, Allmendinger et al. 1983), surficial processes (Montgomery et al. 2003), precipitation and erosion (Abele 1989). This region was chosen because of the interesting and as yet unexplored change in relief around 35° (Figure 2.2), as well as it envelops the region being studied by Gosse, Baker, and Antinao. Several characteristics

other than peak height further support the multi-aspect transition at ~35°'S. Interpretation of the zones determined by characteristics such as relief, basin hypsometry, longitudinal profiles, drainage area-slope information, and tributary asymmetry further supports the interconnectedness of tectonic processes and surface processes put forth by Lamb and Davis (2003).

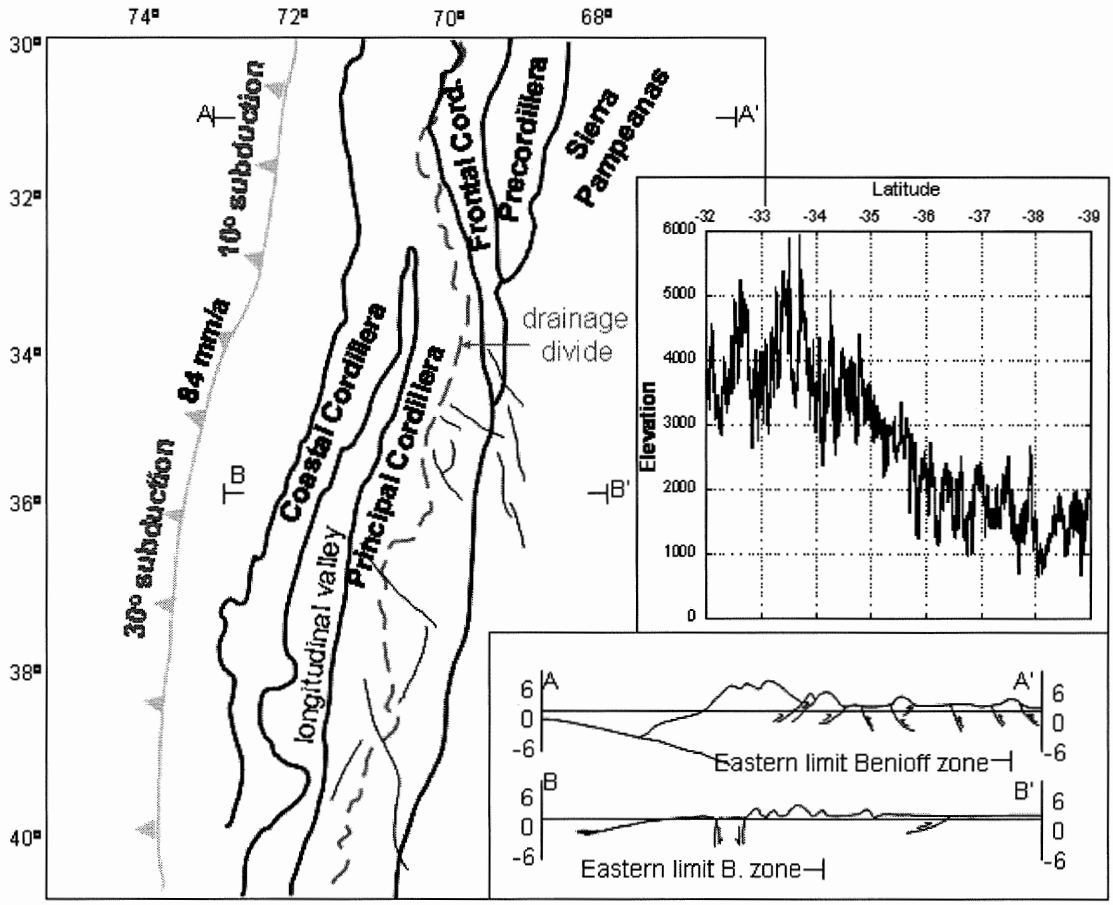

Figure 2.2 Structure and geology of the Andes, from latitude 32° to 39°S (figures from Kennan 2000 and Jordan et al. 1983). Top inset is the elevation profile of the study area, from north to south. Bottom inset are two cross sections which show the change from thick-skinned, shallow subduction and wide Benioff zone in the north, to thin-skinned, steeper subduction and narrow Benioff zone in the south.

Andean tectonics has been extensively studied between 18° and 40°S, where plate subduction is laterally segmented into steep and shallow slabs. It is debated that these segments are separated by a sharp tear (Barazangi and Isacks 1979, in Jordan et al. 1983),

a sharp contortion of the plate (Hasegawa and Sacks 1981 in Jordan et al. 1983), or gradually change dip angle (Kennan 2000). It is also debated that the structures paralleling the strike mirror these tectonic changes (Jordan et al. 1983). The number of ranges changes from five north of latitude 35° (Cordillera Oriental, Cordillera Exoriental, Subandean belt, Coastal Cordillera and Principal Cordillera), to two south of 35° (Coastal Cordillera, Principal Cordillera) (Markgraf 1987). A longitudinal valley, not seen elsewhere in the Andes, separates these two ranges. The Sierras Pampeanas lie east of the magmatic arc above the flat segment of the subducting plate and consist of a series of high, discontinuous, north-trending mountain blocks surrounded by wide flat basins (Allmendinger et al., 1983). The width of the Andes also changes from 50 km in the north to 900 km south of 35° (Markgraf 1987).

Chapter 3.

Methods

3.1 Approaches of DEM Acquisition and Analysis

3.1.1 DEM Source and Attributes

Digital elevation maps from 32° to 39° S, and from 68° to 72° W were acquired from the USGS, Online Seamless Data Distribution System of the Shuttle Radar Topography Missions (http://seamless.usgs.gov/). All maps have horizontal resolution of 3 arcseconds (nominal spatial resolution of 90 m) on a Universal Transverse Mercator projection, and vertical resolution of 1 m (Fig. 3.1). RiverTools provides strike-perpendicular relief swaths, stream area-slope plots, profiles of north-south trending and east-west trending streams, antecedent streams, basin attributes and hypsometries, tributary asymmetry, and drainage divide determined by the DEM along the orogen.

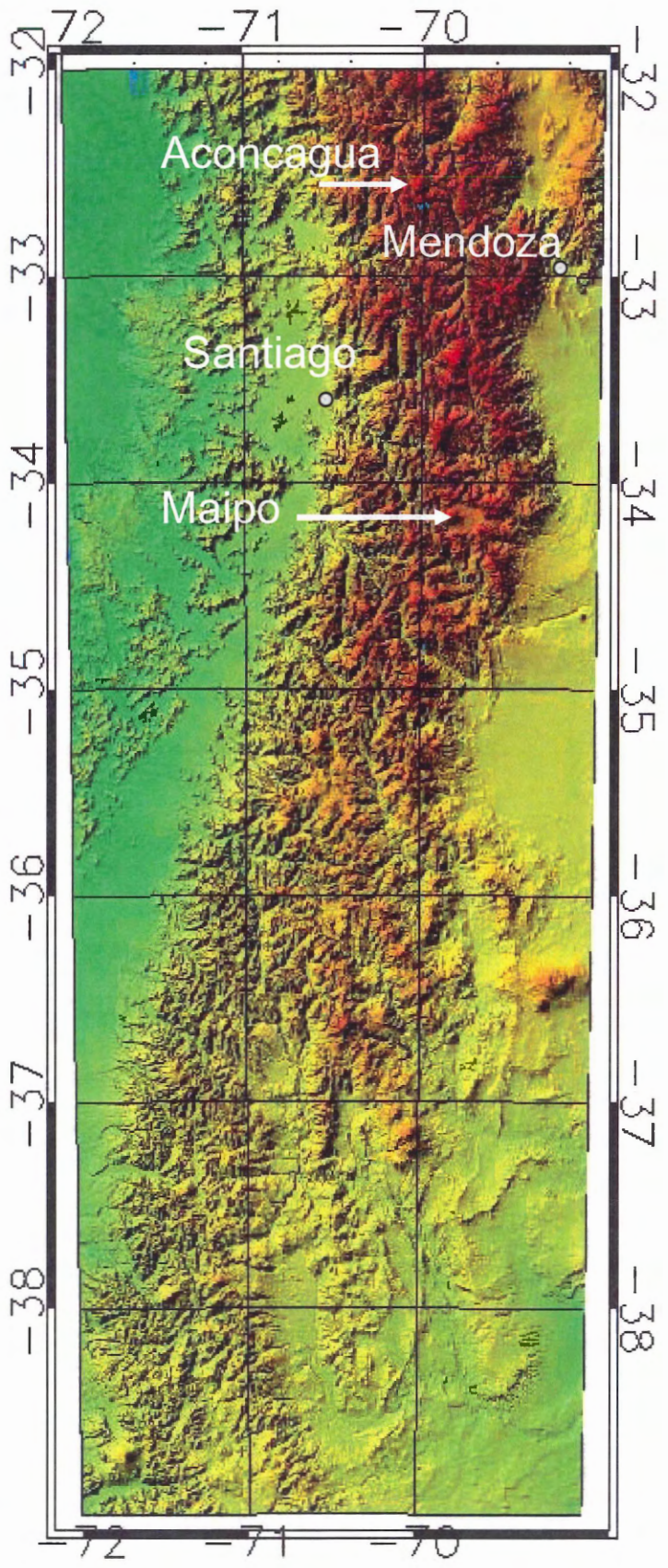

Figure 3.1 Digital elevation map of the transition zone in the southern-central Andes, with major cities and mountains identified. Image has a vertical

3.1.2 DEM Difficulties

DEMs acquired from the SRTM contain areas <40 km^2 in high elevation regions where data is unavailable. These cells register sea level elevation, and affect elevation profiles in several swaths and basin analyses. The effect of these errors is minimal relative to the scope of the entire study area. Smaller areas of no data are averaged by the program, providing an adequate estimation of elevation over that region. DEMs were not seamless in basin analysis. Streams in some basins were truncated at latitudinal or longitudinal boundaries. This required the basin to be carefully analyzed in sections to minimize error. Visualization of hypsometric analysis of basins is limited to cumulative distribution function (CDF) style curves due to a RiverTools error in the display of percentage hypsometric curve plotting.

3.1.3 RiverTools

RiverTools (version 2.4) is a powerful GIS application specializing in the analysis of digital terrain, watersheds and river networks. In basin and topographic analysis, it provides a number of different methods to manipulate data and present results. The application was created by Research Systems, Inc., copyright © 1999-2002, Rivix LLC.

3.2 Geomorphometric DEM-based Topographic Analysis

3.2.1 Methods for determining relief

Relief, the difference in elevation between a local maximum and a local minimum in the topography, is measured at various scales depending on the type and magnitude of the analysis. The difficulty in measuring relief is associated with the three-dimensional aspect of relief itself: how is it possible to measure the variations in the elevation of topography which change in every direction? In essence all measurements of relief are in some ways misleading, insofar as they measure only in one dimension. Two methods were chosen in this analysis to measure different aspects and scales of relief. The latitudinal relief transect method is based on straight line elevation profiles at 1/10° intervals through the entire study area. This method uses small scale (<500 m) "windows" in the topography to find north-south trends in relief and also any shifts in the location of the center of the range. The basin relief method considers the change in elevation between the basin outlet at the mountain front and the peak elevation of the basin at the drainage divide. This method uses a larger topographical window and provides a large scale measurement of relief along the range, and on both sides of the range. Using these methods does not provide a quantitative measurement of the relief of the mountains, but identifies trends in small and large scale relief through the range.

3.2.2 Latitudinal relief transect method

The line profile tool was used to create approximately strike-perpendicular elevation profiles from 32° to 39° S. These swaths were used to visualize and calculate changes in elevation and relief along the strike of the Southern Andes (Fig. 3.2 b.). Elevation profiles were used to calculate relief by extracting peak heights and valley depths (Fig. 3.2 a). By integrating the peak and valley heights over the length of the profile, it was possible to provide a value for relief for each swath. A strike-parallel profile of the length of the mountain chain provided visualization of changes in elevation.

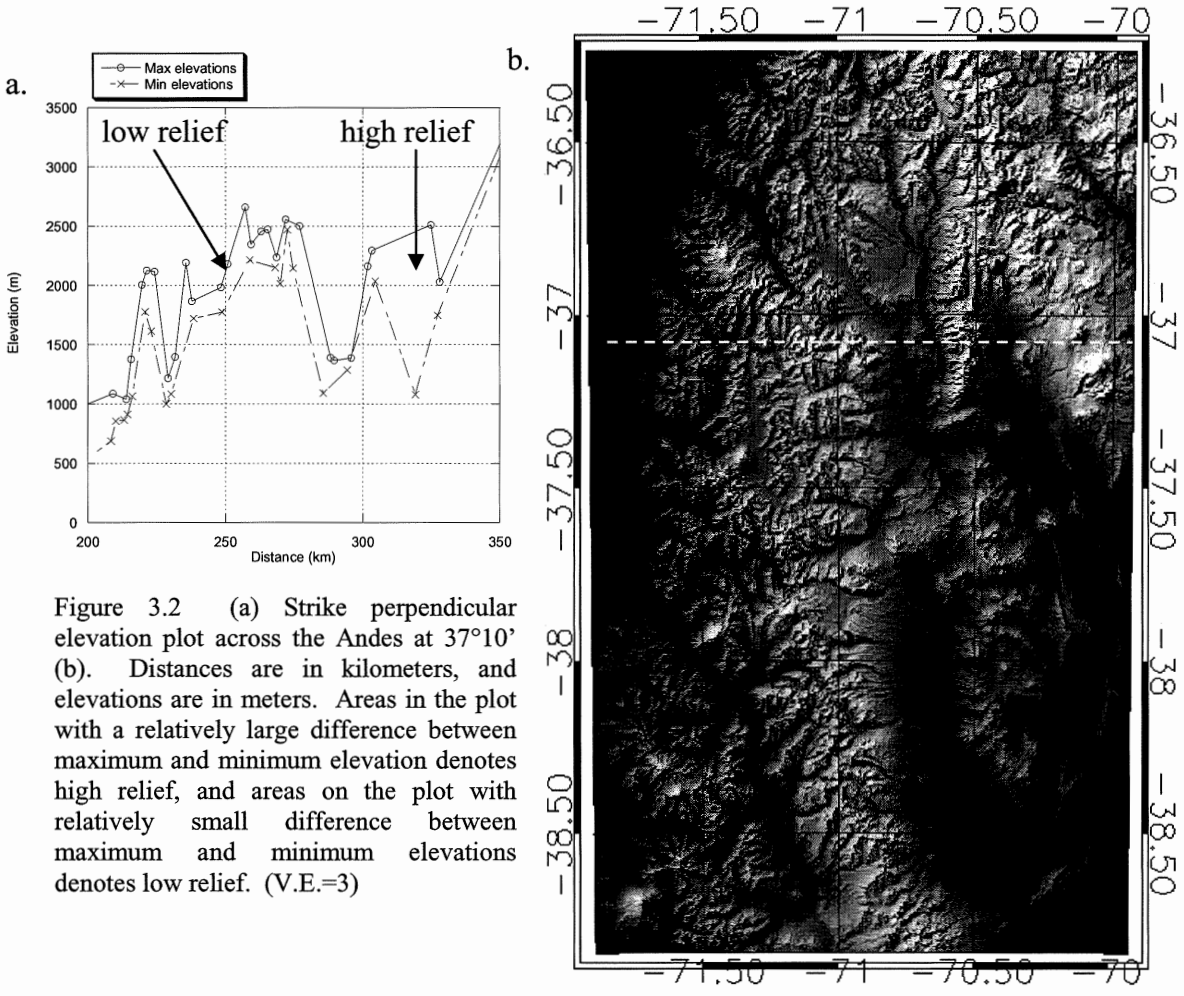

Figure 3.2 (a) Strike perpendicular elevation plot across the Andes at 37°10' (b). Distances are in kilometers, and elevations are in meters. Areas in the plot with a relatively large difference between maximum and minimum elevation denotes high relief, and areas on the plot with relatively small difference between maximum and minimum elevations denotes low relief. (V.E.=3)

3.2.3 Analysis of Drainage Basins

Drainage basins are defined by a main channel, tributaries, and a drainage outlet (Fig 3.3) (Keller and Pinter 2002). Basins were chosen on the basis of the position of the basin outlet relative to the highest elevation of the basin (Fig 3.4). Appropriate basins are large enough to extend from the mountain front to the center of the range, which provided a datum to compare all basins. Basins are characterized by outlets at the mountain front, and peak elevations at or near the drainage divide. The drainage divide for this portion of the Andes is defined by the edges of the drainage basins on the east and west flank of the mountains. The study area was divided into 23 basins, which cover the majority of the area of the mountain front. Basins range in size from 649 km^2 to 8283 km^2, with an average of 2484 km^2.

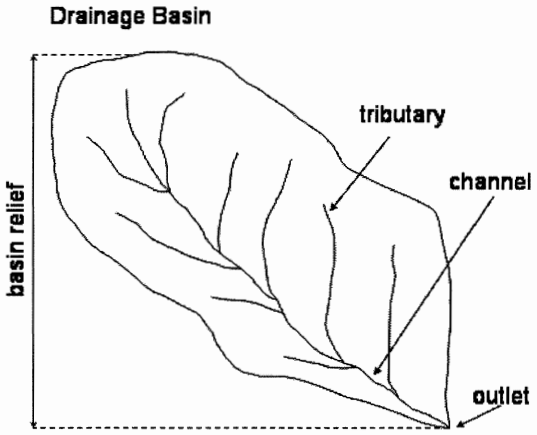

Figure 3.3 Features of a drainage basin. Basins are bowl-shaped catchments defined by the drainage divide (outline), channels and tributaries, and an outlet. Basin relief is the change in elevation between the outlet and the highest point in the basin.

In order to produce a basin outlet, the software requires a flow grid, a treefile, and a river network. The river network is structured by Strahler stream order, which assigns the smallest tributaries the value 1, and increases the value when two same-order streams meet. RiverTools then provides a list of attributes for each basin, including outlet coordinates, basin area, relief, Strahler order of the dominant channel, network diameter, longest and total channel length, drainage density, and finally normalized CDF hypsometric curves and hypsometric integrals for each basin.

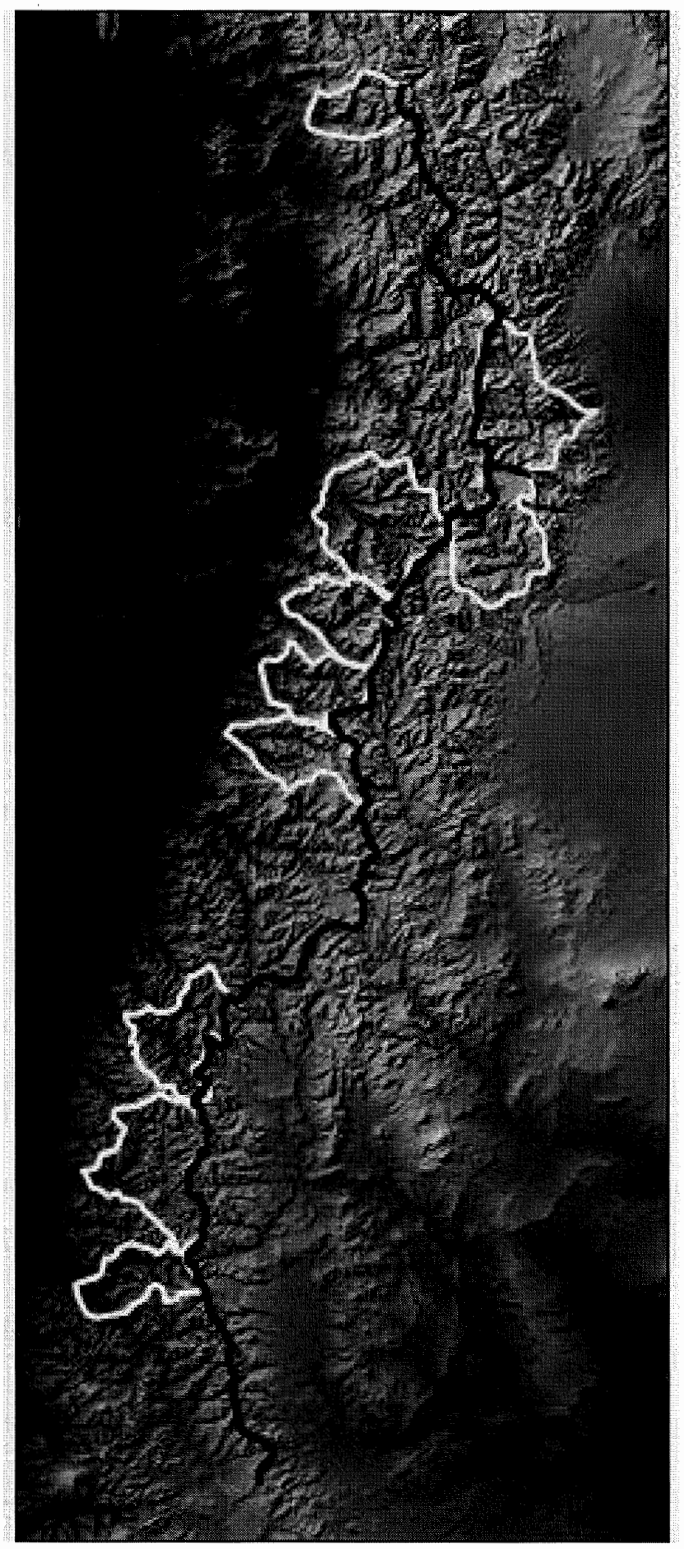

Figure 3.4 Drainage basins for the Andes between 32° and 39°S latitude. Image is a DEM shaded relief, with masked regions of the basins, and the drainage divide in black (V.E.=3). Basins were chosen on the basis of data completeness and spatial range (from mountain front to continental divide).

3.2.4 Longitudinal Profiles of Streams

Channel profiles plot the along-channel distance against channel elevation, from the point of maximum elevation to the channel outlet (Fig 3.5). Channel profiles of strike-perpendicular streams determine possible migrations of the drainage divide (Keller and Pinter 2002, Hovius 2000). Channels of Strahler order 5 or greater were chosen for this analysis, and long profiles were truncated at the outlet. Channel concavity has been shown to be related to the maturity and stability of the channel in an environment that is not tectonically controlled (Hovius 2000). Concavity was measured using an exponential function as an approximation for the profile and also by using the area between the channel profile and a linear upper limit to the profile.

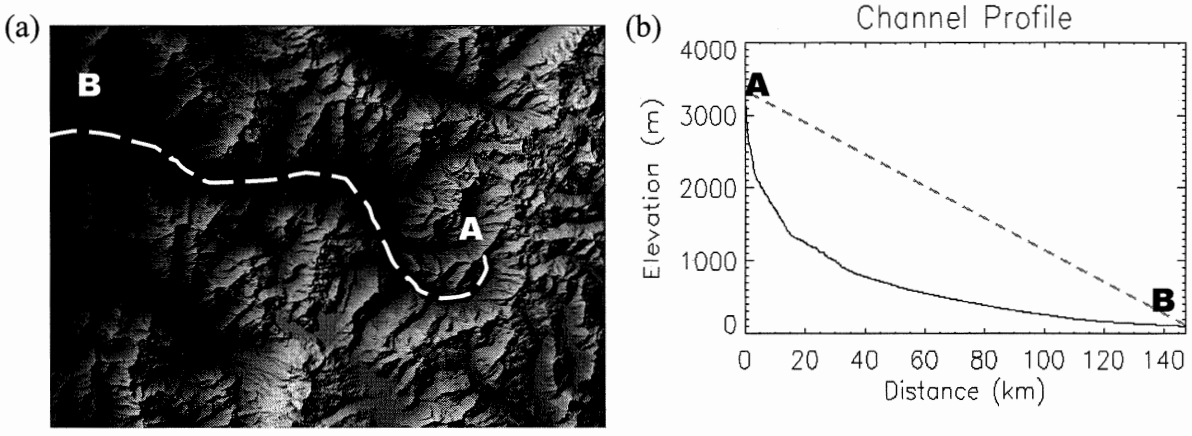

Figure 3.5 Example of longitudinal profile. (a) DEM (V.E.=3) of the Rio Teno in Chile (34.8°S, 71°W), which flows east to west and (b) the longitudinal profile of this river which shows a steeper slope in the eastern reaches of the river and a shallower slope in the western reaches near the outlet.

3.2.5 Tributary Length Asymmetry

Tributary analysis of streams shows how differences in the lengths of tributaries can indicate the presence of differential uplift (Fig 3.6). East-west trending channels with north-south trending tributaries reveal changes in uplift in the north-south direction (Keller and Pinter 2002). North-south trending channels reveal changes resulting from east-west uplift. Eighteen channels trending east-west were chosen, with lengths from 25.0 to 81.4 km (average 45.3 km). Nine channels trending north-south were chosen with lengths ranging from 27.6 to 118.9 km (average 56.0 km). Stream order ranged from 4^{th} to 6^{th} order, depending on the magnitude of the channel.

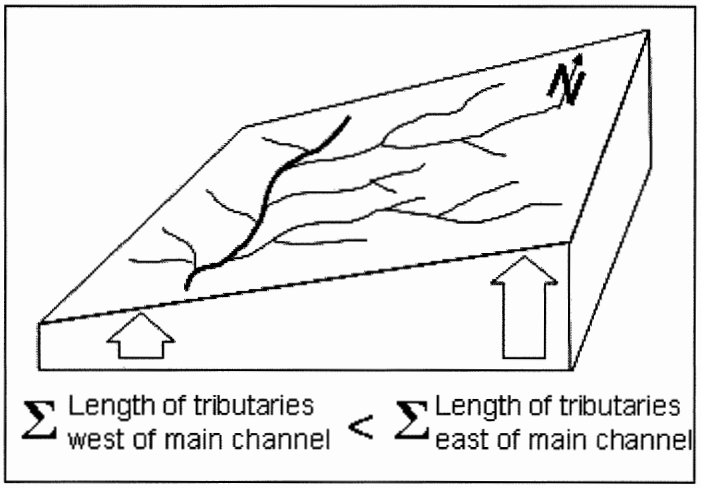

Figure 3.6 Schematic diagram showing tributary asymmetry. From Keller and Pinter, Prentice Hall, 2002. The arrows show proportional uplift and the resulting stream length asymmetry produced in a basin on the surface.

3.2.6 Mountain-front sinuosity

Mountain front sinuosity is a measure of the balance between erosional forces creating wide valleys along the mountain front, and tectonic forces which create straight lines along the mountain front (Keller and Pinter 2002) (Fig 3.7). The index uses the ratio of the mountain front at some predetermined scale, and the straight line length of the mountain front. A mountain front with sinuosity close to one may be along a fault or

some other active tectonic structure. A large value signifies dominantly erosional forces are smoothing out rolling hills which are not tectonically active (Keller and Pinter 2002). It is important to realize the importance of scale using this index. A large scale will not consider smaller variations in the mountain front, but a small scale will produce high values for on all mountain fronts. The relative increase or decrease in the sinuosity of a mountain front is considered in this analysis, using a scale of measurement of 3 km over straight line sections of 50 km.

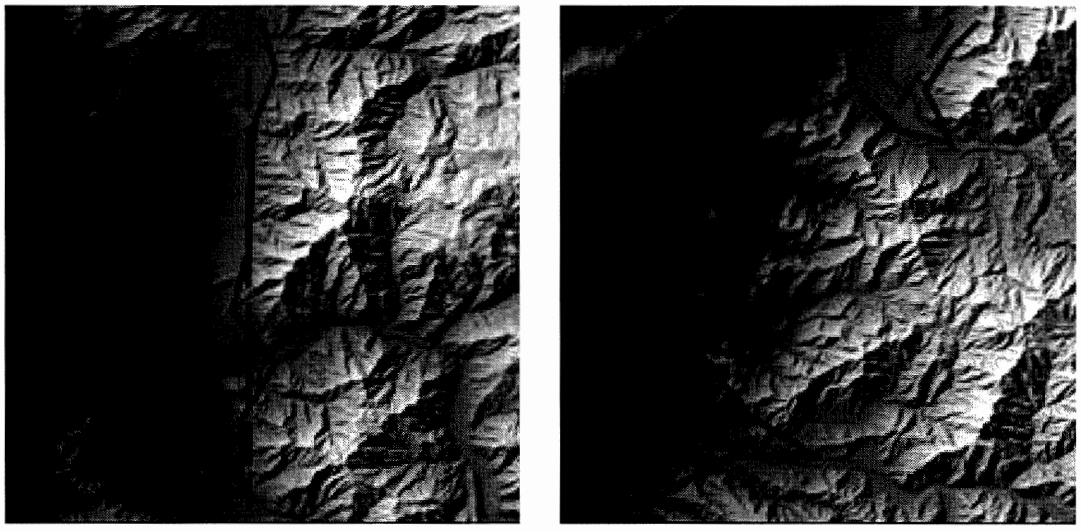

Low sinuosity, $L_{mf}/L_s \sim 1$ Higher sinuosity, $L_{mf}/L_s > 1$

Figure 3.7 Example of the determination of two different mountain front sinuosity values. The size and scale of the DEMs are the same, the dashed line is the straight length of the mountain front segment, and the solid line is the length of the actual mountain front. Mountain front length accuracy is limited to the resolution of the measurement "yard-stick". In this case, resolution was 3 km therefore any valleys along the front with width less than 5 km were measured as straight line lengths. (V.E.=3)

3.2.7 Area-slope Analysis

Area slope analysis is a descriptive method which can predict whether a stream will be alluvial or bedrock judging by its slope and drainage area. If we assume a stream is at equilibrium over extended time scales, in other words there have been no major events which have caused the basin to shift stream slopes or drainage area then a pattern should be evident in the distribution of stream order with respect to drainage area and slope. Sklar and Dietrich (1998) studied the longitudinal profiles of documented rivers and the known processes of incision associated with each river and plotted them in a diagram (Fig 3.8) by drainage area and channel slope. Field data suggests there are four regions of finite slopes where fluvial processes, bedrock exposures and active channel incision ca n be expected to occur (Sklar and Dietrich 1998).

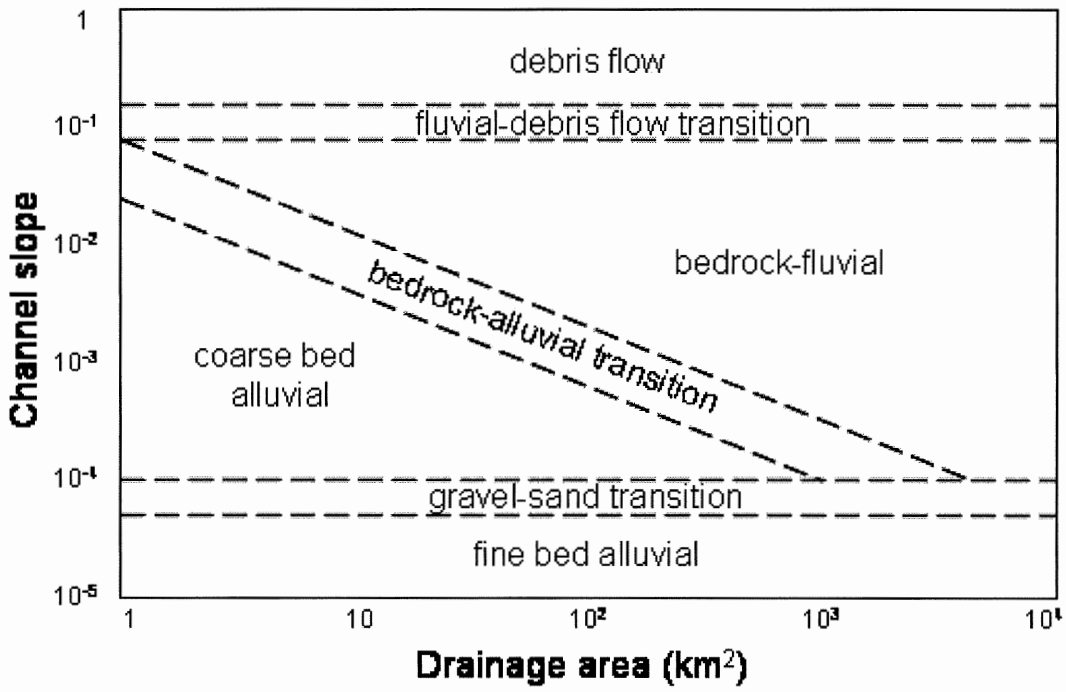

Figure 3.8 This figure shows fields of dominant fluvial processes relating to the slope and drainage area of a stream. Taken from Sklar and Dietrich, 1998. Lines represent approximate upper and lower bounds of dominant process transition zones.

Figure 3.9 is an example of the complete data set of tributaries, an x-y plot, for one basin along with Skar and Dietrich's (1998) diagram. RiverTools provides x-y plots which code each tributary segment by strahler order where cyan = 1st order, green = 2nd order and so on. This data shows several important relationships: Lower order streams have a wide range of slopes in small drainage basins while higher order streams have consistently lower slopes and higher drainage area. Low to moderate order streams are equally probable to be alluvial streams or mass wasting streams, while higher order streams are more likely to be bedrock stream. Using an area-slope analysis, it may be possible to determine trends in upper order areas or slopes, as well as identify other relationships.

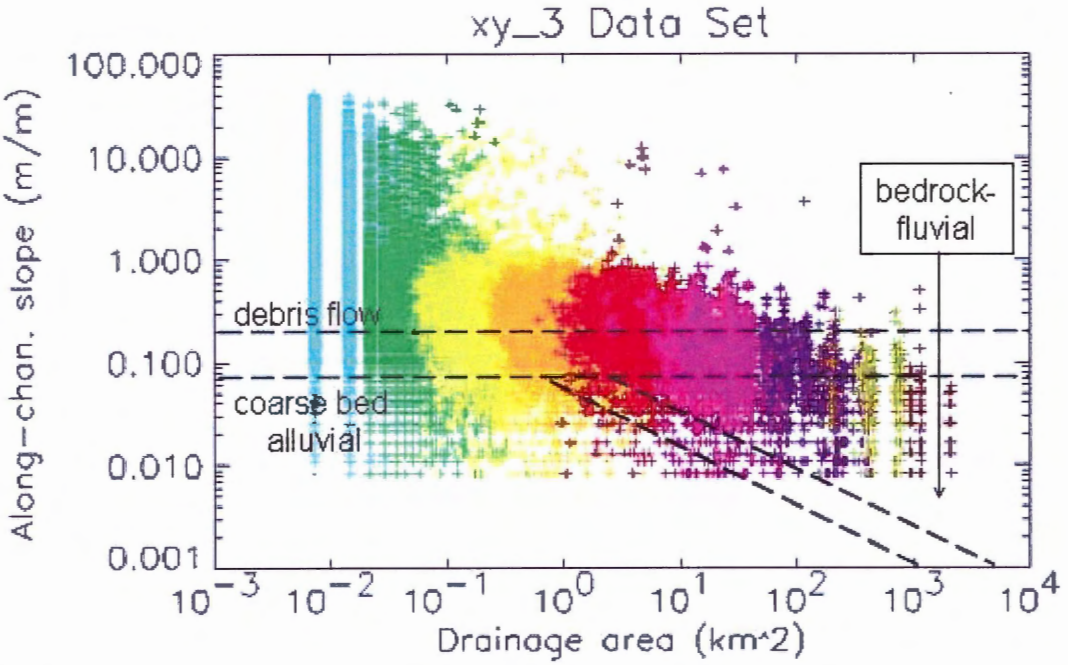

Figure 3.9 Area slope analysis of a stream in the study area. Each cross represent one reach of a stream in the basin. The colors represent strahler stream order, from lowest order (cyan=1st) to highest order (deep red=10th). In most steams, low order streams have high slopes and low drainage area while high order streams have low slope and high drainage area.

The area-slope analysis is limited by the program in that it extracts slopes which are solely greater than 0.01 m/m hence the region of fine bed alluvial processes is not seen. From this diagram, we can determine that the dominant process of steep, smaller streams is debris flows, and that the dominant process of high order streams is bedrock erosion. A sharp decrease in slope occurs from 2° streams (slopes = 1-120 m/m) to 3° streams (slopes <1m/m) for this basin. The results from this analysis will compare relative erosive processes between adjacent basins.

3.2.8 Analysis of topographical change

A drainage divide is defined as the boundary of the catchment basin, or the areal limit of drainage of a basin (Burbank and Anderson 2001). From 32° to 39°, the divide was determined using the overlapping boundaries of basins reaching from the mountain front on the east and west flanks. It is important to understand the evolution of the divide and the surrounding streams with respect to the basins and channels which define it. Antecedant streams, one which maintains its course throughout periods of uplift and deformation, describe the paleotopography and can give information about how paleoflow has changed over time. They are generally strike parallel to the mountain chain, such as in the northwest of this image.

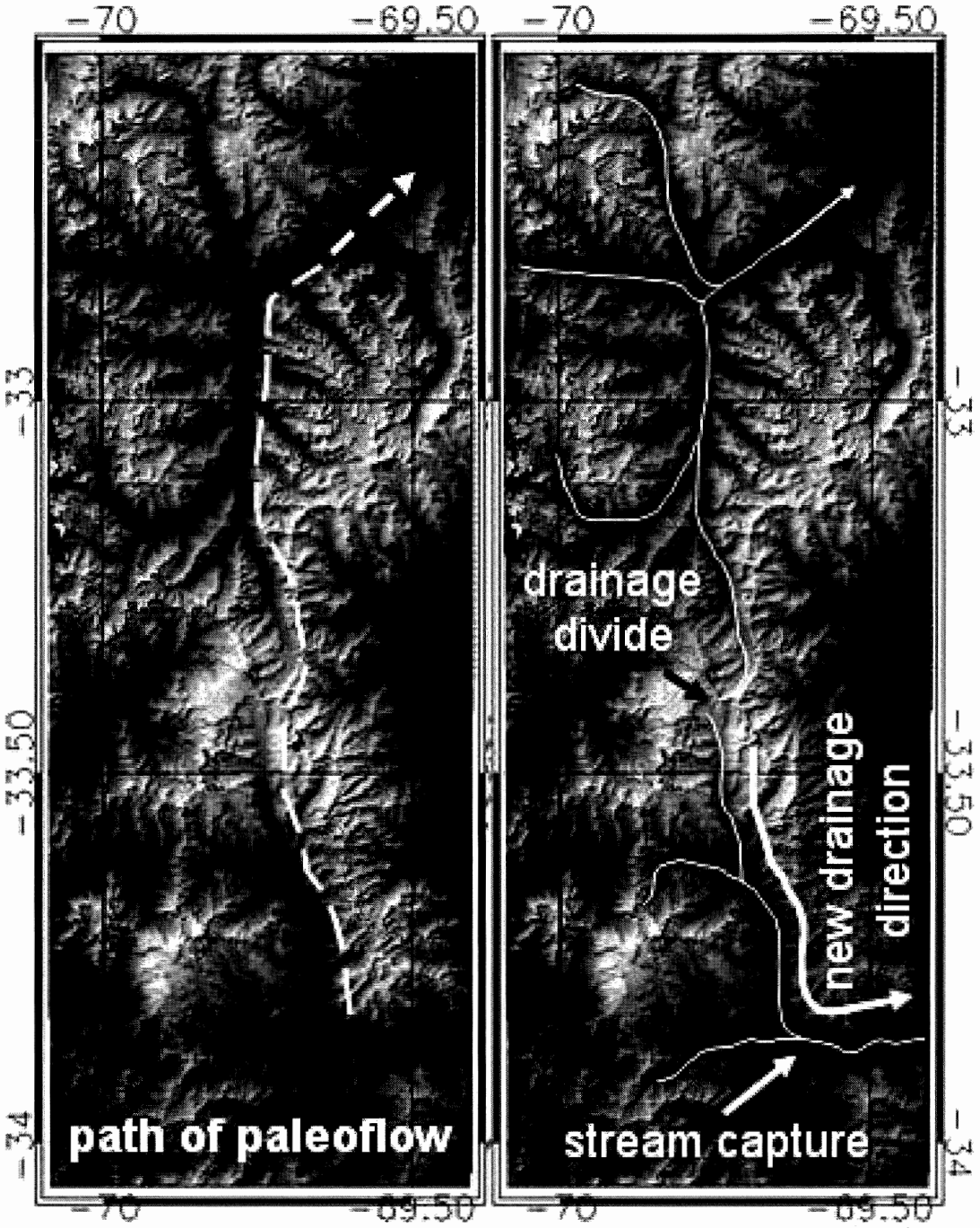

Figure 3.10 Example of how paleoflow can be determined by examining features such as antecedent streams. The DEM on the left shows two longitudinal streams which suggest that paleoflow in this region once ran south to north. In the north, rivers drain into the Rio de los Palas and in the south rivers drain into the Rio Tunuyan. Mount Tupungatito is located at the drainage divide. The DEM on the right shows that the present day flow of these streams has changed to two streams separated by a drainage divide. A possible explanation for this feature is uplift in the area of the drainage divide. (V.E.=3)

Chapter 4.

Results

4.1 Relief

4.1.1 Latitudinal transect relief

Relief is the difference in height between an interfluve crest and the adjacent valley floor. As mentioned in chapter 3, relief can be difficult to measure in a meaningful way because it varies spatially. Using the latitudinal transect relief method, the area between 32°S and 34.5°S latitudes exhibits relatively high relief. The maximum relief in this region ranges from 4036 m to 5320 m. In some cases this relief is constrained to high elevations regions (the high peaks of the Principal Cordillera) (32°, 32.5° and 34°, Fig. 4.2), but in other places high relief occurs along the flanks of the Andes. Latitudes 35° to 36.5° show the first indication of moderate relief, and further south relief varies from moderate to low. Maximum elevation decreases from 4210 m at 35°, to 3570 m at 36°, to 3016 m at 36.5°S. At 35° the width of the range is the narrowest relative to the rest of the study area. The transect along 33.5° exhibits the highest elevation in the study area. However as indicated in Fig. 4.2, this is not the average for that latitude. The plot of elevation (a) shows a highly undulating topography with high peaks and low valleys for the first 200 km of the north-south transect. This section includes the region of the Aconcagua (6958m) and the Tupungatito (6569m) mountains. The average relief from 32° to 35° is 430.7 ± 108 m. Relief decreases abruptly at 35° and averages 189.2 ± 76.3 m from 36° to 39°.

a.

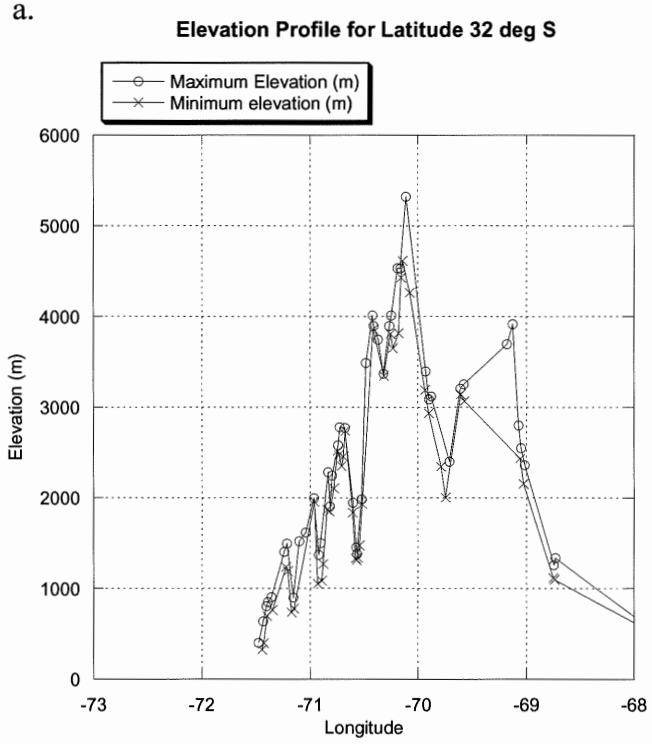

b.

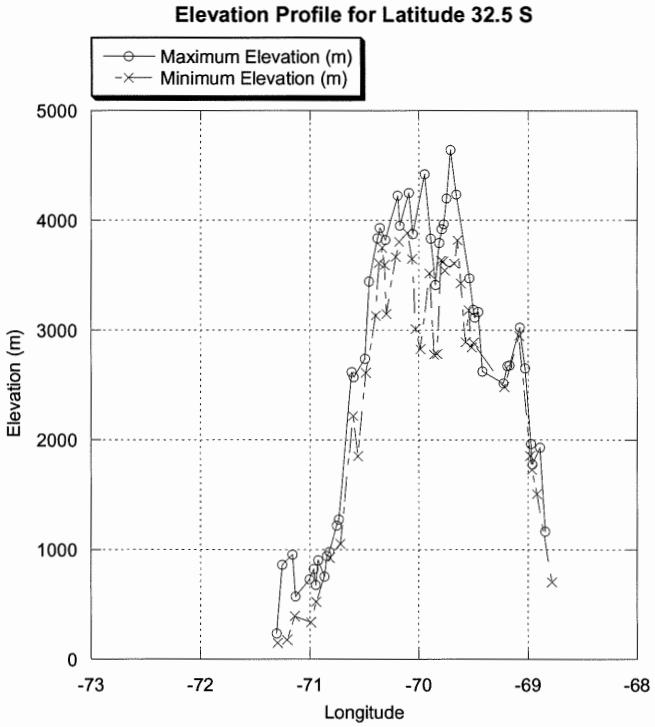

Figure 4.1 (a) and (b) Elevation profile for latitudes 32 and 32.5°S.

c.

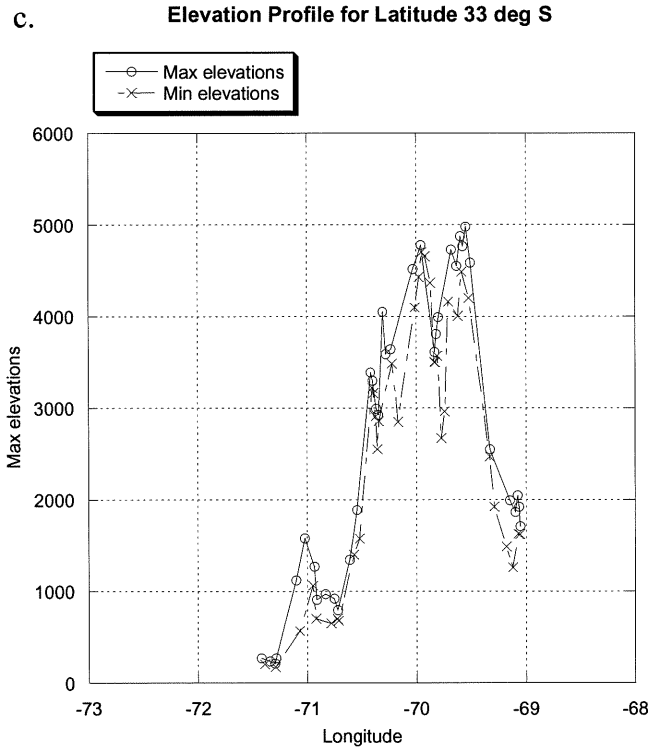

d.

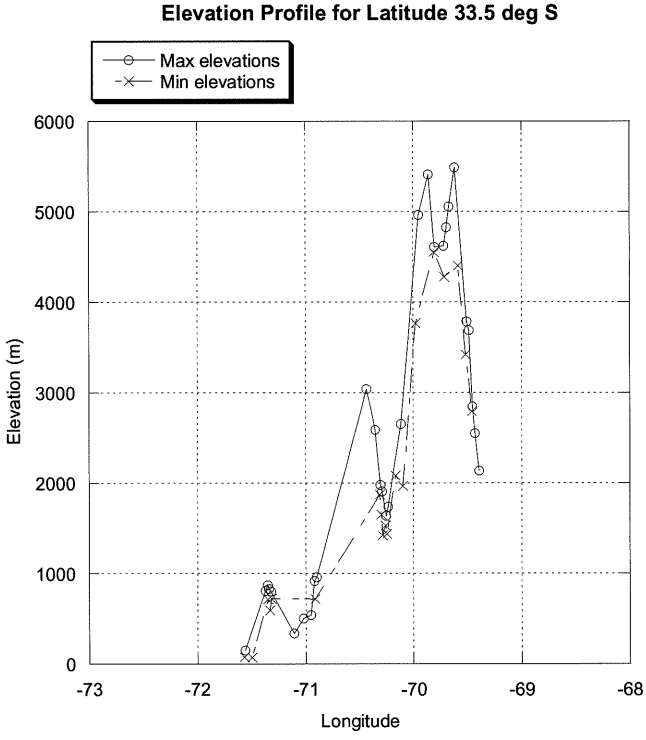

Figure 4.1 (c) and (d) Elevation profile for latitudes 33 and 33.5°S.

e.

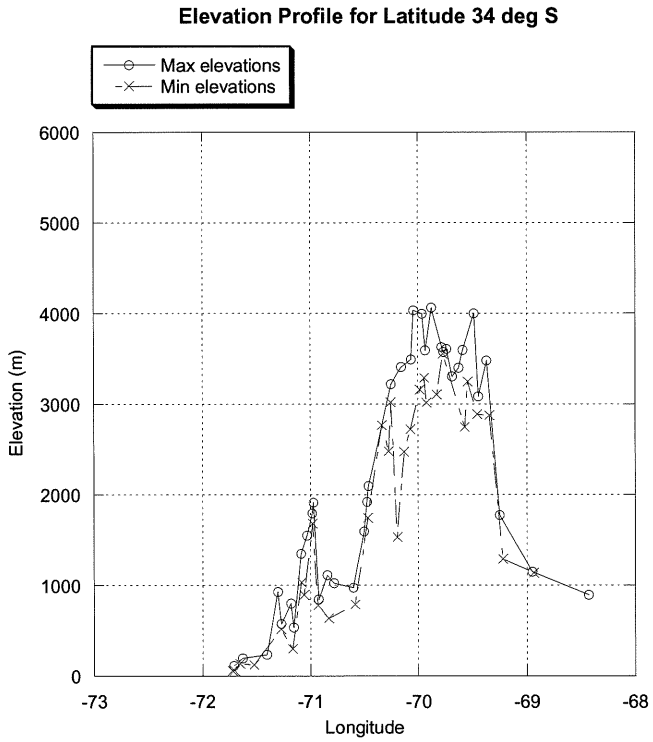

f.

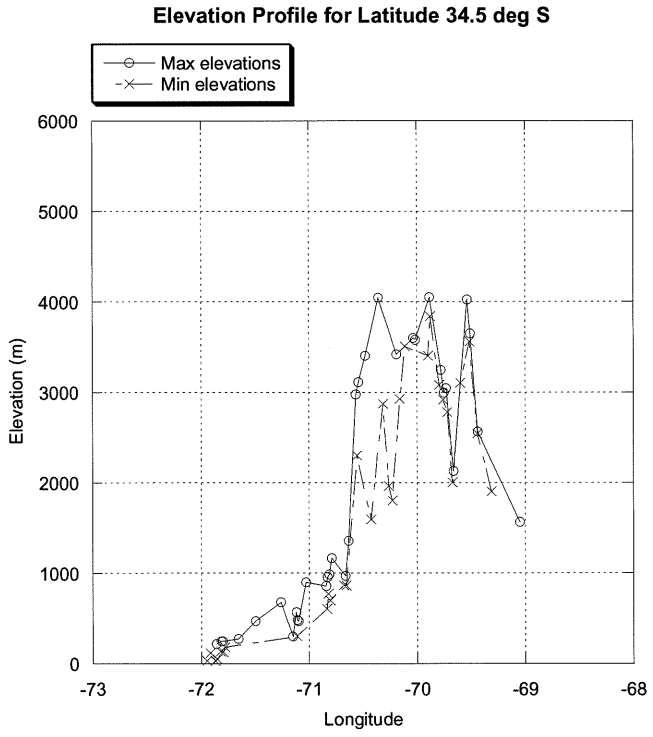

Figure 4.1 (e) and (f) Elevation profile for latitudes 34 and 34.5°S.

g.

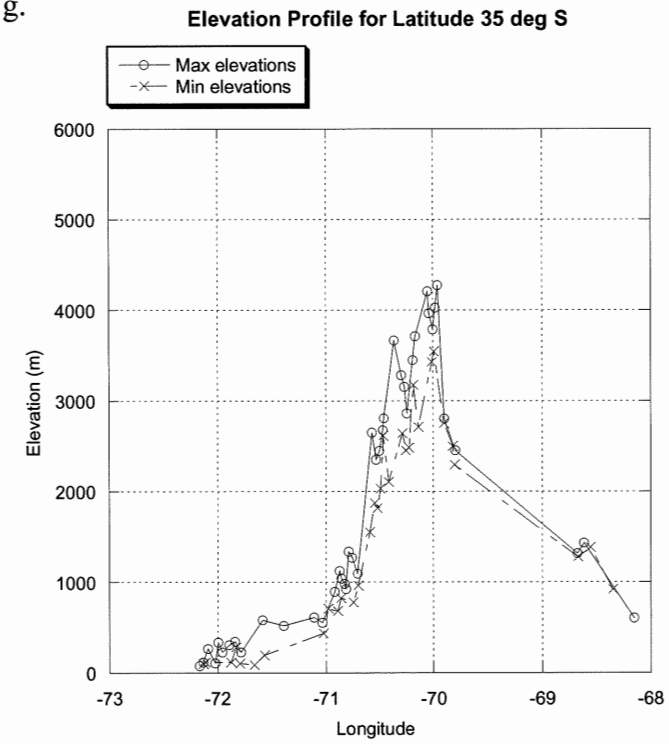

h.

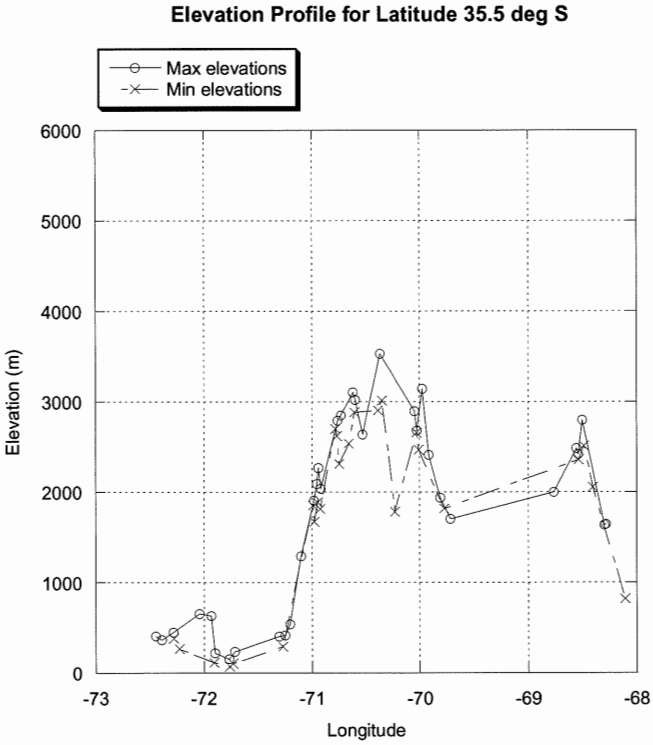

Figure 4.1 (g) and (h) Elevation profile for latitudes 35 and 35.5°S.

i.

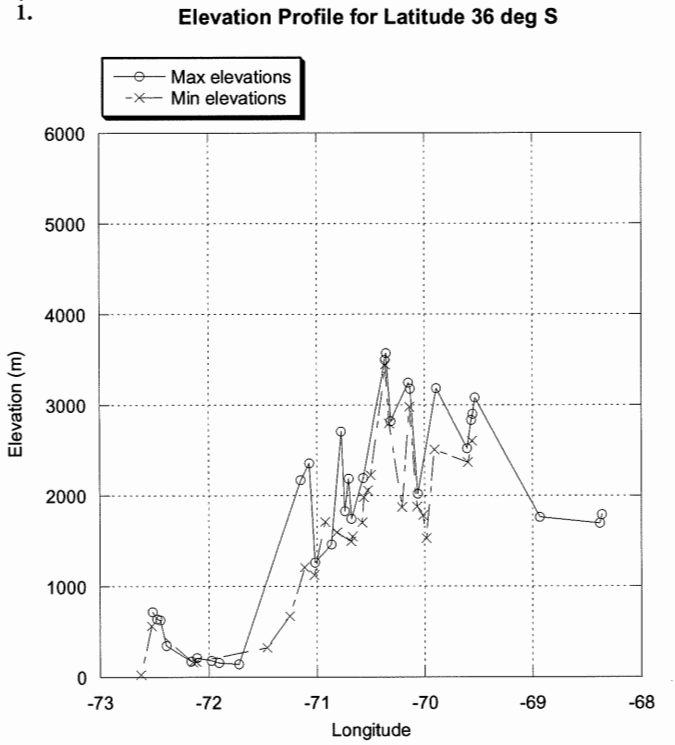

j.

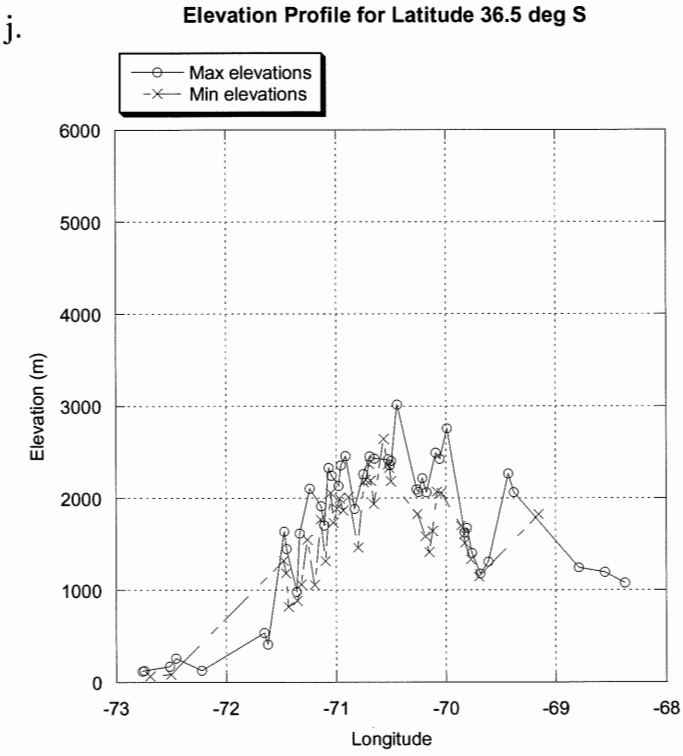

Figure 4.1 (i) and (j) Elevation profile for latitudes 36 and 36.5°S.

k.

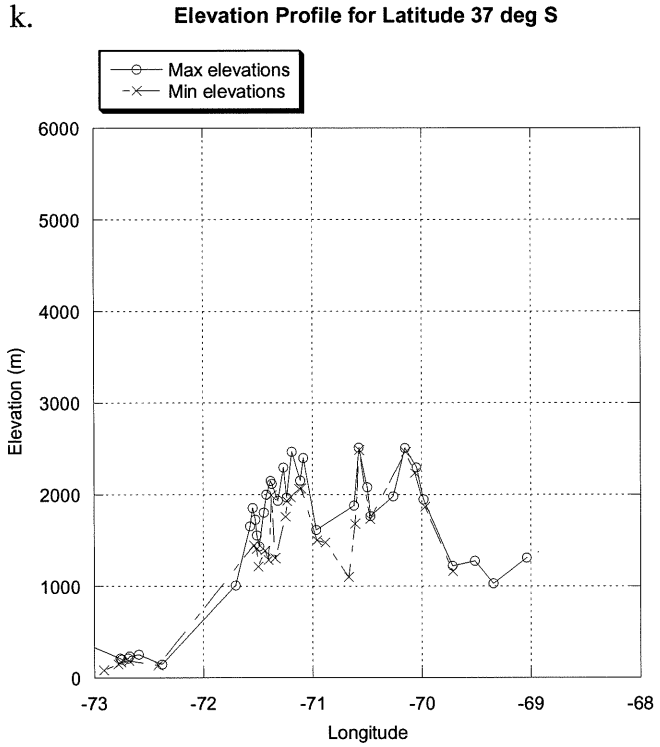

l.

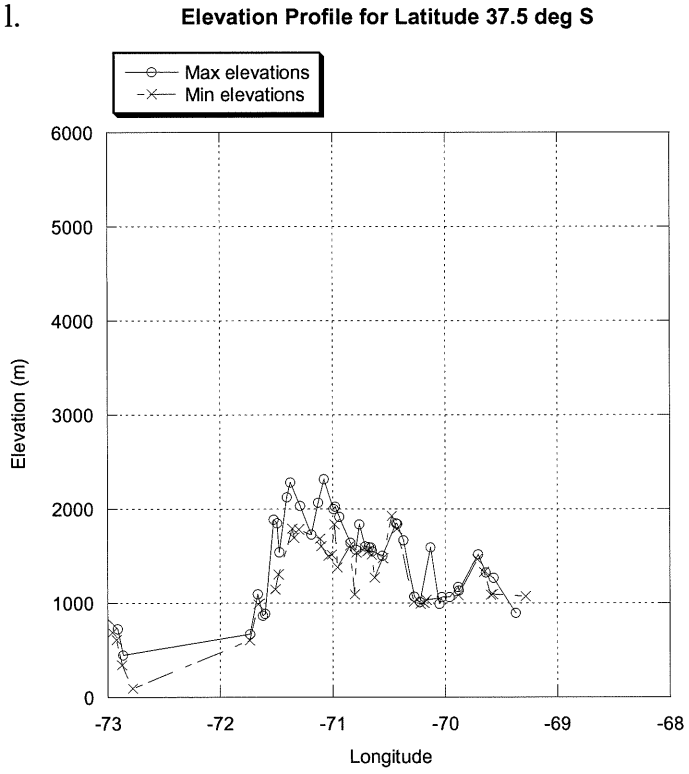

Figure 4.1 (k) and (l) Elevation profile for latitudes 37 and 37.5°S.

m.

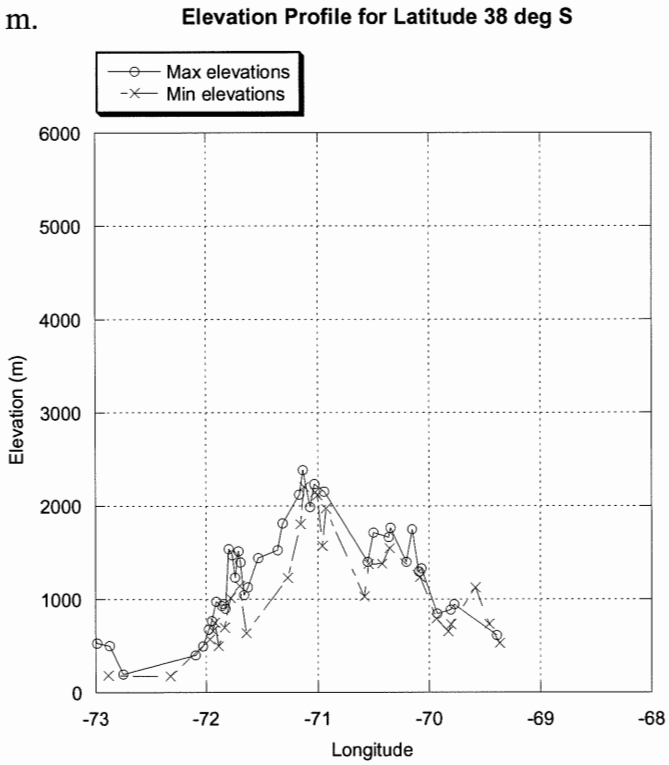

n.

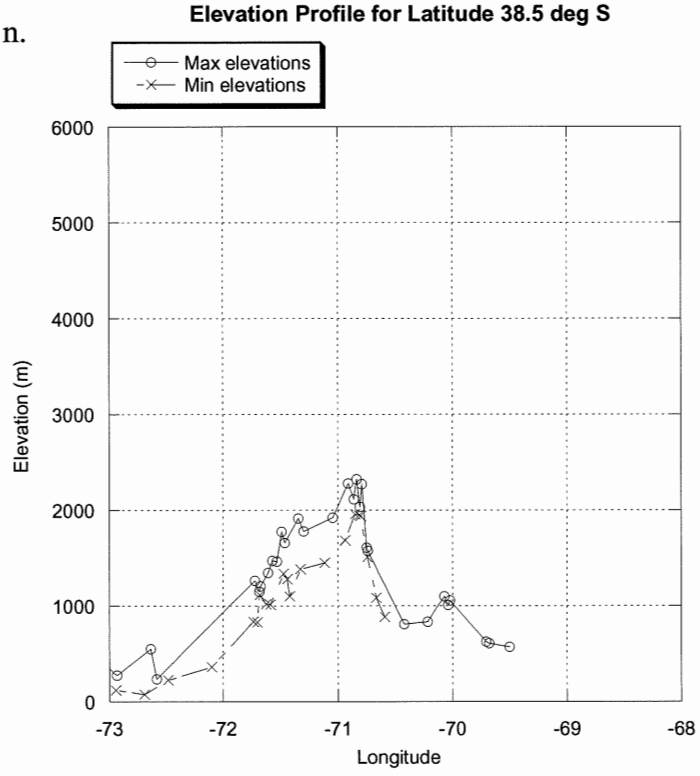

Figure 4.1 (m) and (n) Elevation profile for latitudes 38 and 38.5°S.

o.

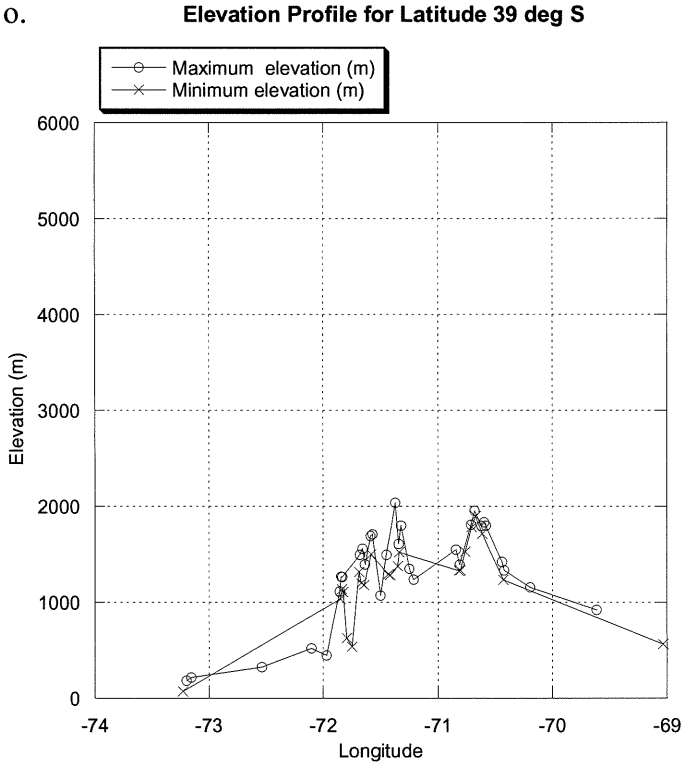

Figure 4.1 (o) Elevation profile for latitudes 39°S.

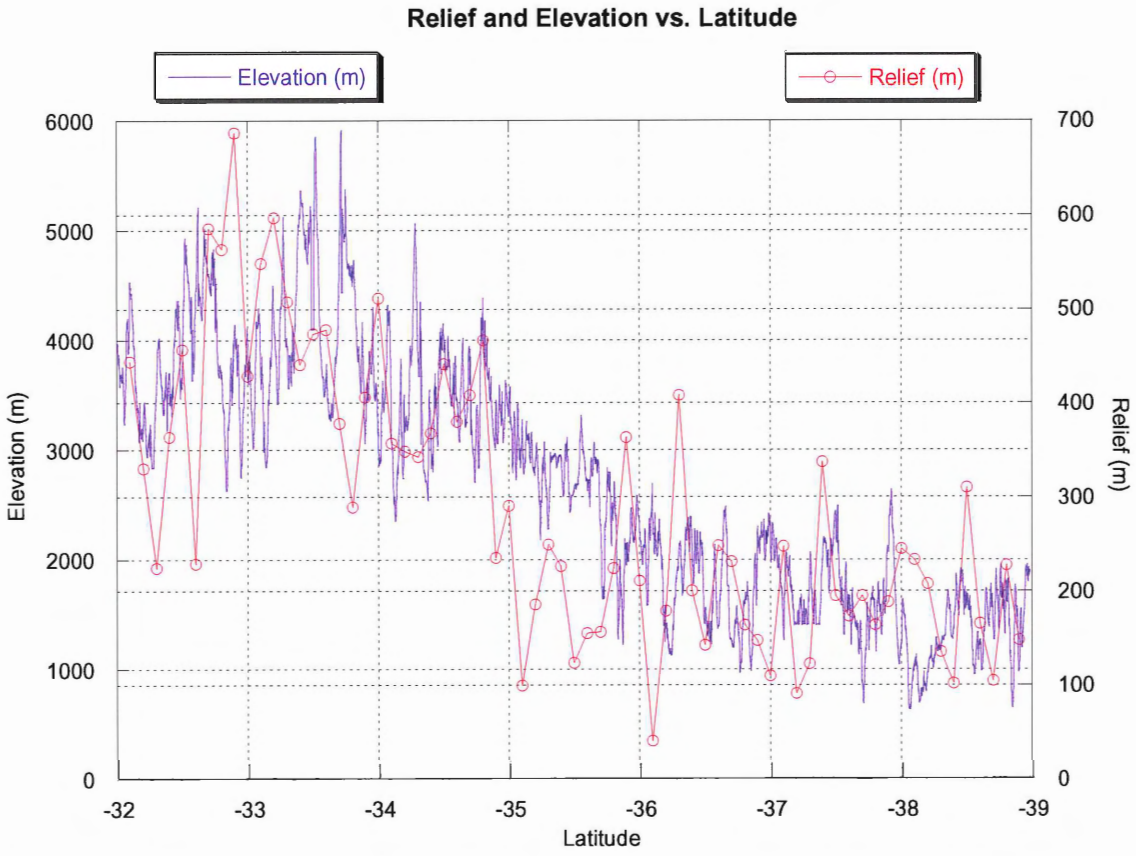

Figure 4.2 (a) Elevation and relief (red with circles) of the Andes along strike from 32° to 39°S (blue). Relief was determined using the method described in the appendix, table 1. Elevation of the range was determined using a straight line transect along the highest peaks, which in many instances mimics the continental divide.

4.1.2 Basin Relief

Basin Relief was calculated for 17 basins using the vertical difference between the elevation of the outlet and the peak elevation of the highest strahler order stream in the basin. Basin relief was determined by normalizing these values to the smallest relief value. The purpose of normalizing the data was to emphasize the relative change in basin relief in all of the basins. Basin relief values ranged from 2.5 km to 4.8 km, with decreasing values towards the south (Table 4.5). Drainage basins were chosen on the basis of their size relative to the range itself. The outlets lie on the mountain front, and the basin extends to the drainage divide of the range. The drainage divide defined by basins on the east and west side of the Andes (solid line) are in agreement with the divide determined by Jordan et al (1983). Basin sizes range from 639 km^2 to 8283 km^2 however basin area was not a factor in relief, in accordance results found by Strahler (1952) and Keller and Pinter (2002). Truncated basins formed by an error in the DEM were omitted from the analysis.

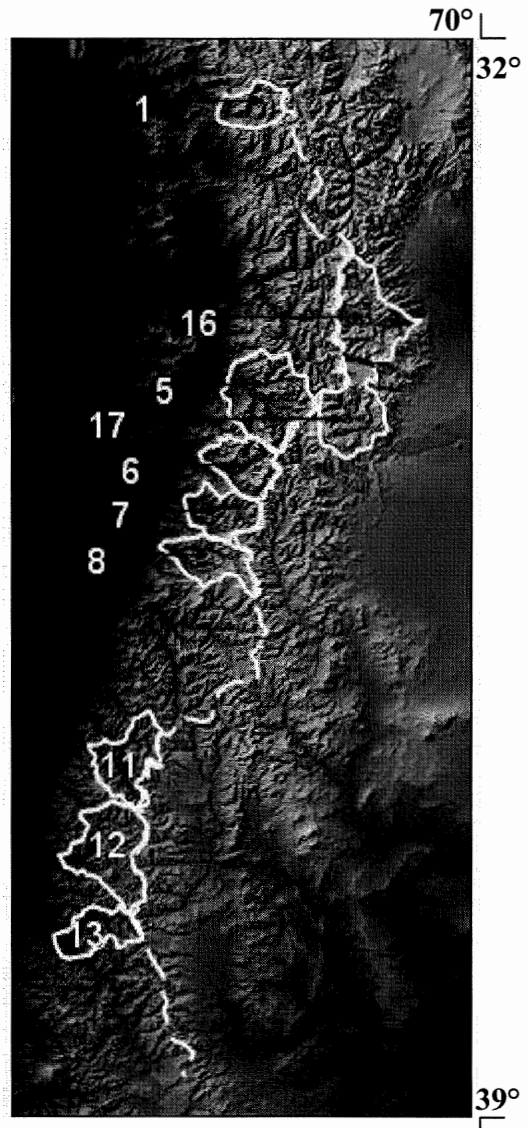

Figure 4.3 Outline of drainage basins in the study area, chosen by the breadth of the basin- from drainage divide to the mountain front. Basins excluded from this anaylsis were truncated at latitudinal or longitudinal boundaries by the processing software. (V.E.=3)

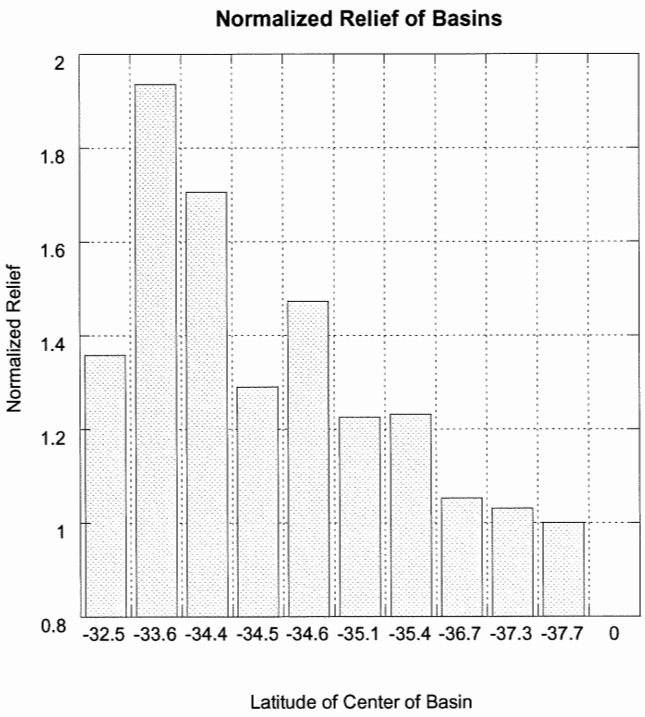

Figure 4.4 Relief of basins from figure 4.3, plotted by latitude, normalized to the relief of the basins with the least relief (found at 37.7°S).

Outlet Number	Information	Outlet coord.	Basin Relief (m)
1	Outlet at La Ligua	-70.678, -32.553	3395
16	Including Rio Tunuyan	-69.387, -33.865	4837
5	Outlet at Rancagua	-70.610, -34.267	4262
17	Including Rio Diamante	-69.580, -34.587	3223
6	Outlet at San Fernando	-70.762, -34.739	3682
7	Including Rio Teno	-70.871, -34.985	3061
8	Including Rio Colorado	-71.003, -35.282	3078
11	Including Rio Nuble	-71.479, -36.608	2631
12	Including Rio Antuco	-71.708, -37.319	2576
13	Including Rio Bio-Bio	-71.712, -37.773	2499

Table 4.5 Relief of drainage basins defined by the outlined regions in figure 4.3.

4.2 Longitudinal Profiles

In general, longitudinal profiles of streams decrease in gradient monotonically, are concave up with occasional local convexities, and are smooth over length scales of kilometers, excluding the effects of knickpoints (Hovius, 2000). Throughout the study area, streams of various sizes and orientations were chosen to compare stream concavity and hypsometry. Streams of strahler order 8 or larger were chosen on the basis of their length from the drainage divide to the mountain front. These are the largest streams in the study area, and are generally strike-perpendicular. Knickpoints in a river profile are notches in the curve created by differences in resistance of different rock types, or if the channel crosses a fault and uplift has changed the elevation on one side of the fault. Knickpoints can represent a snapshot of a streams response to changes in climate or other factor that cause the stream to slip out of equilibrium (base level changes, sediment flux, and discharge) (Gosse, pers. comm.). Knickpoints are difficult to identify because of the presence of many small discontinuities in the DEM at the kilometer to tens of kilometers scale. Structural changes and changes in lithology along each channel were examined using the Mapa Geologico de Chile (2002) and Mapa de Recurso Minerales del Area Fronteriza Argentino-Chilena (1997).

Stream 2 has a convex bulge in the profile over an area of volcaniclastics ~50km long. A similarly shaped bulge occurs in stream 1a, however geological information was unavailable for the most northern reaches of the study area. The Rio Diamante (stream 7) and Rio Atuel (stream 9) have similar shapes- both have similar slopes in the head of the streams, and also at the mouths of the streams. The Rio Diamante has small convex

notches in the profile where the channels overlie pyroclastic and andesitic rock, and the Rio Atuel has convex notches where the river overlies Jurassic sedimentary rocks. Stream 4 has a very smooth profile, even though it passes over several units of Cretaceous and Jurassic rocks. The Rio Maipo (stream 6) has a small bulge in the profile however rock type is of Quaternary age throughout the channel. The Rio Teno (stream 11) shows a long bulge in the profile where the channel overlies Jurassic sedimentary rocks. The profile for the Rio Colorado (stream 12) is disturbed in the upper reaches where the channel overlies plutonic rocks. The Rio Pueiche (stream 14) overlies volcanic and plutonic rocks, and the Rio Melado overlies volcanic rocks. Both profiles have many notches and bulges which make interpretation difficult. In the Rio Barrancas (stream 16), ~65km from the head of the stream there is a knickpoint in a unit of Miocene-Pliocene volcanic rocks. The Rio Sources (stream 17) lies above volcanic rock, and the Rio Nuble lies over Quaternary sedimentary rocks. The Rio Antuco (19) overlies volcanic rocks in the upper reaches and Quaternary sediments towards the mouth of the river. The steep upper reach of the Rio Agrio (20) corresponds to the edge of a caldera, and the bulge 25km from the head of the channel corresponds to the stream passing through the opposite side of this caldera.

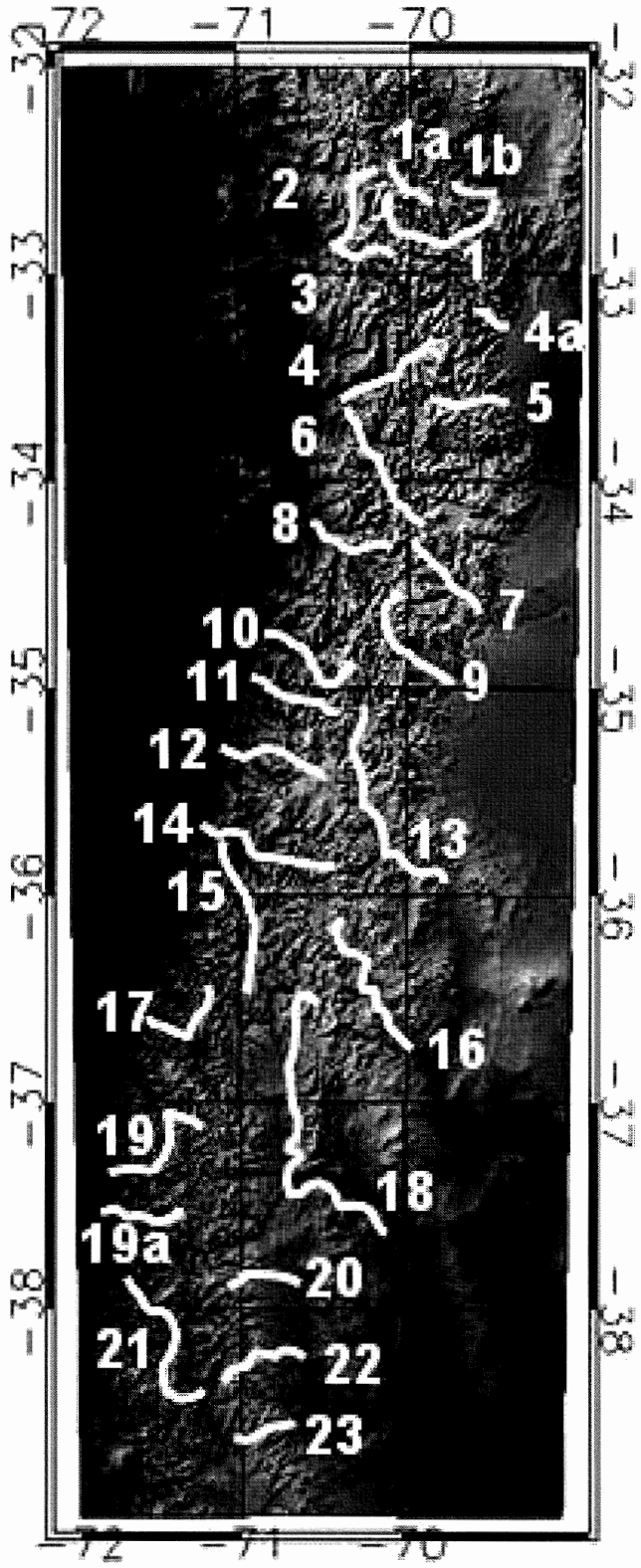

Figure 4.6 Locations of streams used to create longitudinal profiles for analysis using hypsometry, and concavity. Streams were chosen on the basis of orientation relative to the drainage divide (roughly perpendicular), length (from mountain front to drainage divide) and strahler order (>8) (V.E.=3) Stream 1 = stream through Puente del Inca, 1a = western reach of Rio Palas, 1b = stream through Puente del Inca, 2 = northern reach of stream through town of Rio Colorado, 3 = southern reach of stream through town of Rio Colorado, 4 = stream from Cerro Tupungatito, 4a = Rio Anchayuyo, 5 = stream near western road from Tunuyan, 6 = Rio Maipo, 7 = Rio Diamante, 8 = stream flowing NW to San Fernando, 9 = Rio Atuel, 10 = stream flowing NW to San Fernando, 11 = Rio Teno, 12 = Rio Colorado, 13 = upper reach of Rio Grande, 14 = Rio Pueiche, 15 = stream flowing NNE to Talca, 16 = Rio Barrancas, 17 = Rio Nuble, 18 = Rio Neuquen, 19 = Rio Antuco, 19a = stream flowing south of Los Angeles, 20 = northern reach of Rio Agrio, 21 = Rio Bio-Bio, 22 = southern reach of Rio Agrio, 23 = Arroyo Corunco.

a.

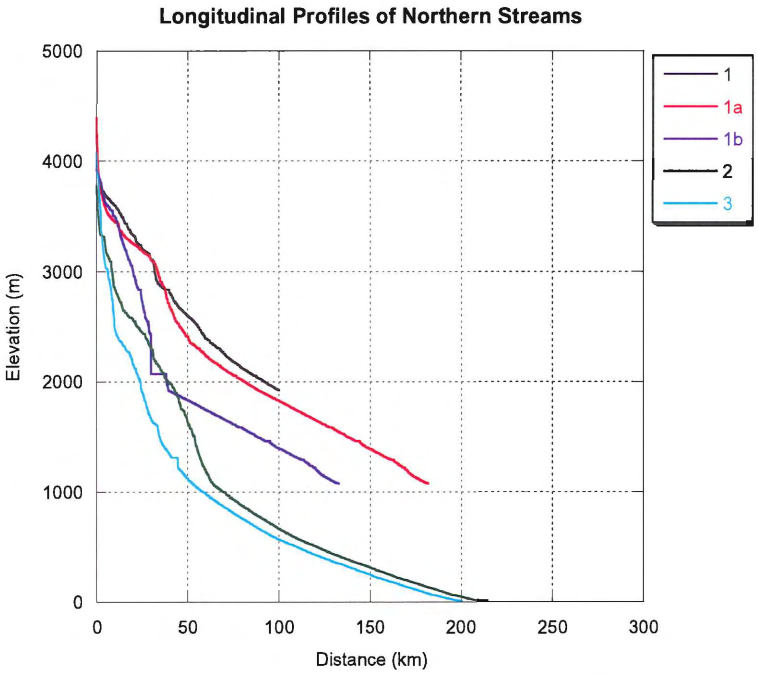

b.

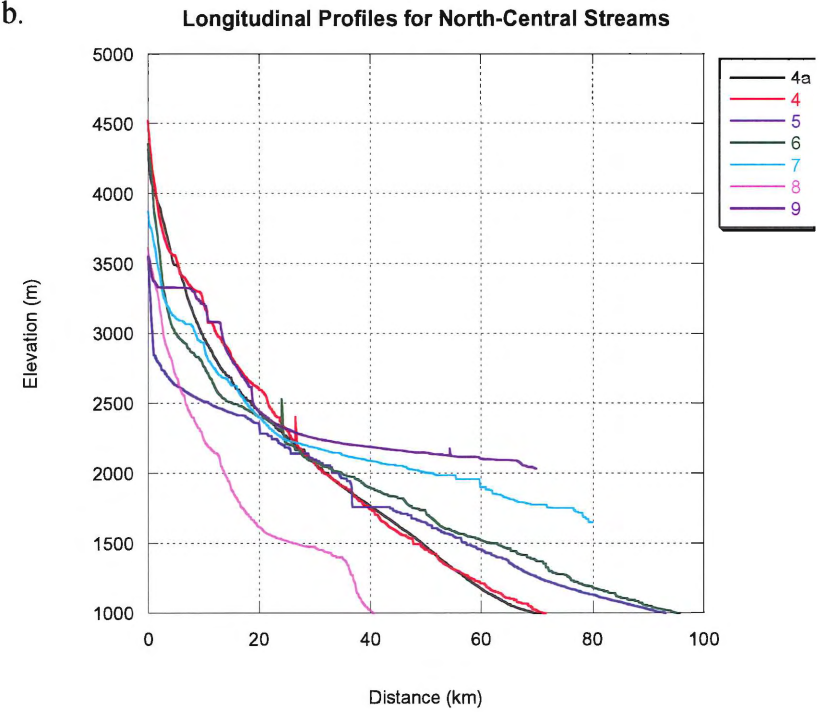

Figure 4.7 Longitudinal profiles of streams with locations outlined in figure 4.5. (a) Streams located in the north, (b) and (c) streams in the central latitudes of the study area and (d) streams in the south.

c.

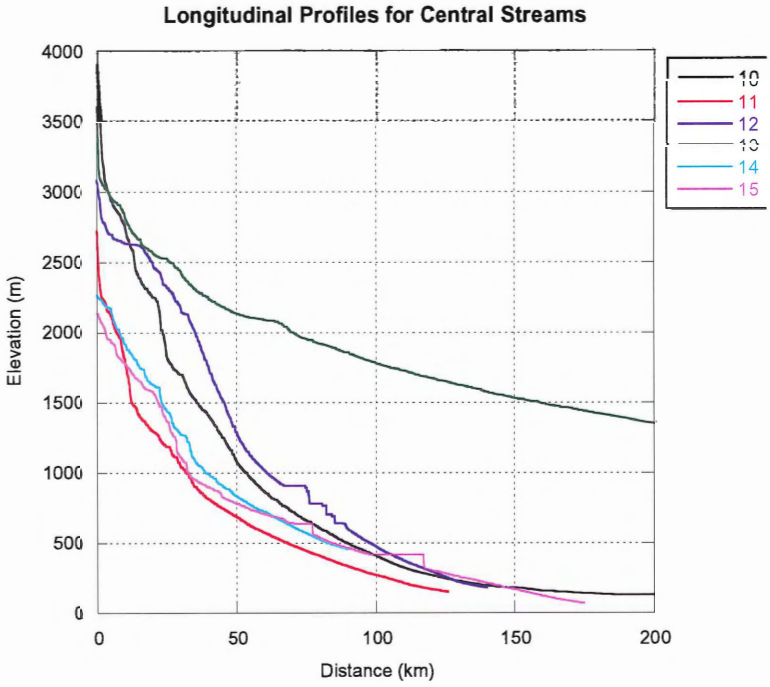
Longitudinal Profiles for Central Streams
Elevation (m)
Distance (km)
10
11
12
13
14
15

d.

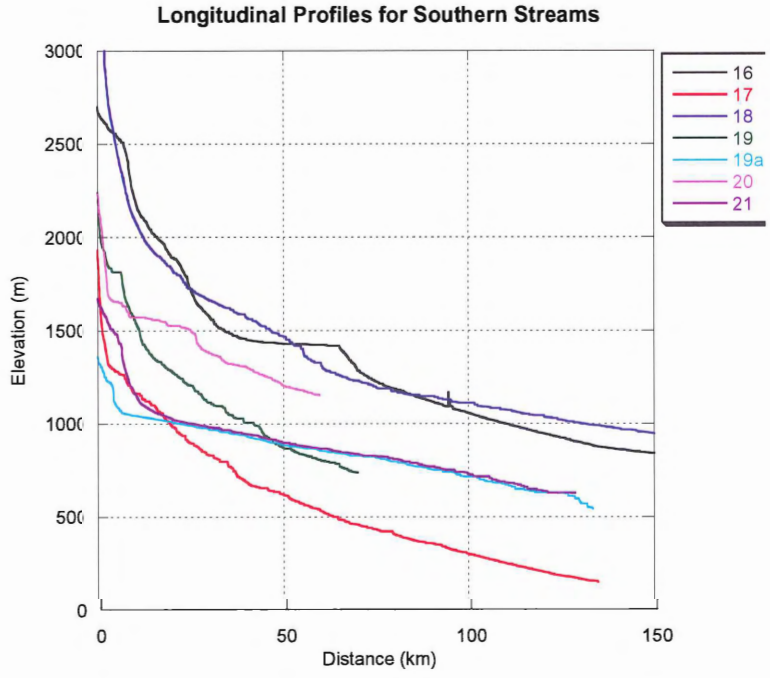
Longitudinal Profiles for Southern Streams
Elevation (m)
Distance (km)
16
17
18
19
19a
20
21

4.3 Concavity

Stream concavity is a measure of the relationships between river bed elevation and downstream distance (Hovius, 2000). In this analysis, concavity was determined using two methods. The first method assigns an exponential decay function to the longitudinal profile and uses the rate of decay as the concavity (Fig 4.8). A high rate of decay represents high concavity, and a low rate of decay represents low concavity (Hovius, 2000). In several streams it was not possible to create an accurate longitudinal profile approximation due to the many inconsistencies in the shape of the profile. The second method measures concavity by finding the area between the profile and a straight line plotted from the head to the outlet of the stream (Fig. 4.10). The methods used to show concavity show two contracting trends. Method 1 shows an increase in concavity from 32° to 36.5°S, with one outlier at 38°S. Method 2 shows a decrease in concavity from north to south. The trend seen in method two is most evident in shorter streams and lower order streams.

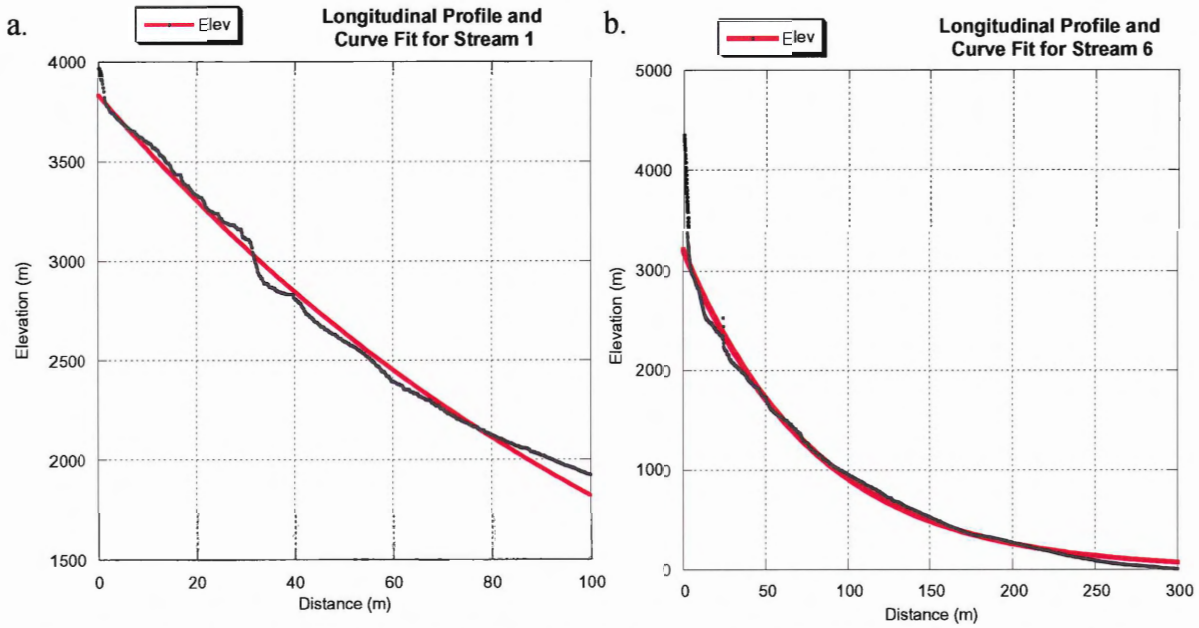

Figure 4.8 Examples of the application of concavity: method 1. (a) unknown stream name (stream 1) with concavity = 0.0074645 and (b) Rio Maipo (stream 6) with concavity = 0.012538. The thin line is the longitudinal profile of the stream and the thick line is the assigned function of exponential decay of the profile.

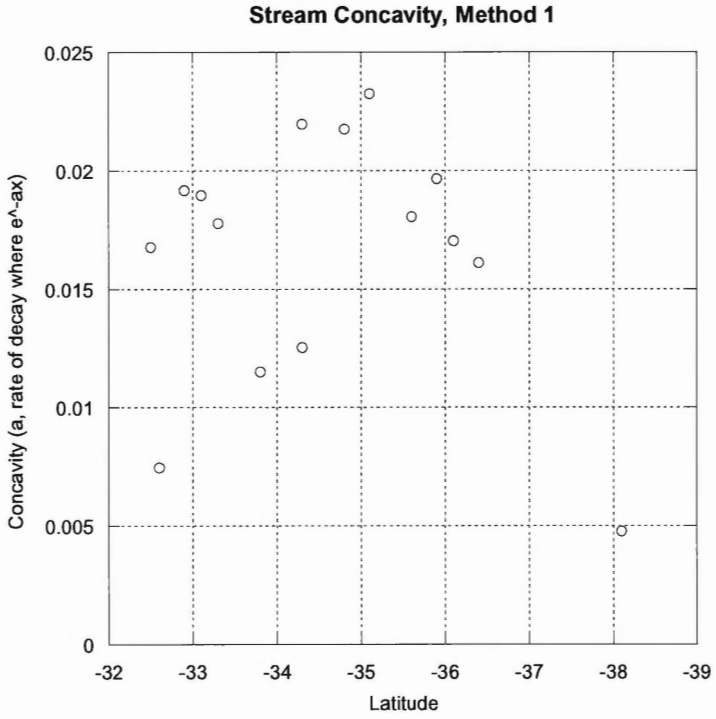

Figure 4.9 Concavity of all streams using method 1 (refer to figure 4.8), plotted from north to south.

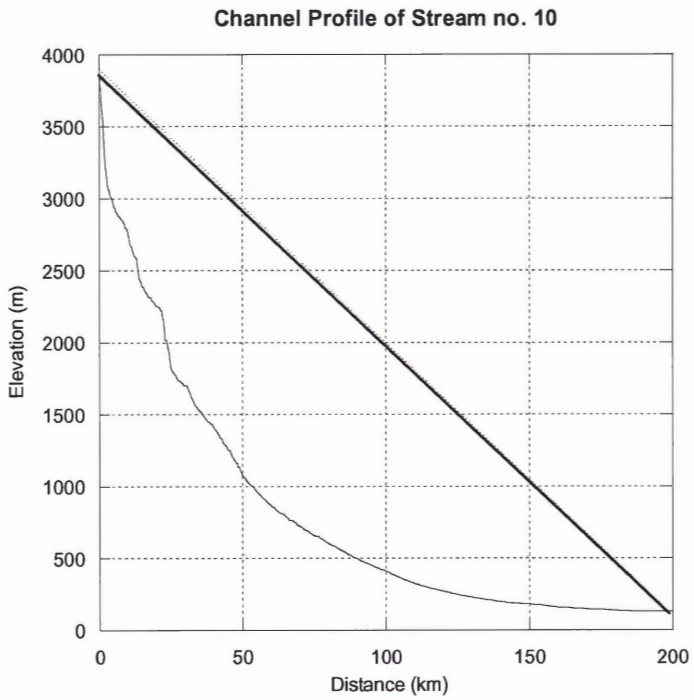

Figure 4.10 An example of the application of concavity : method 2. Stream 10 (name unknown) has a concavity value of 242838 m·km. The area between the channel profile and the line bounding that profile determines the concavity of that channel.

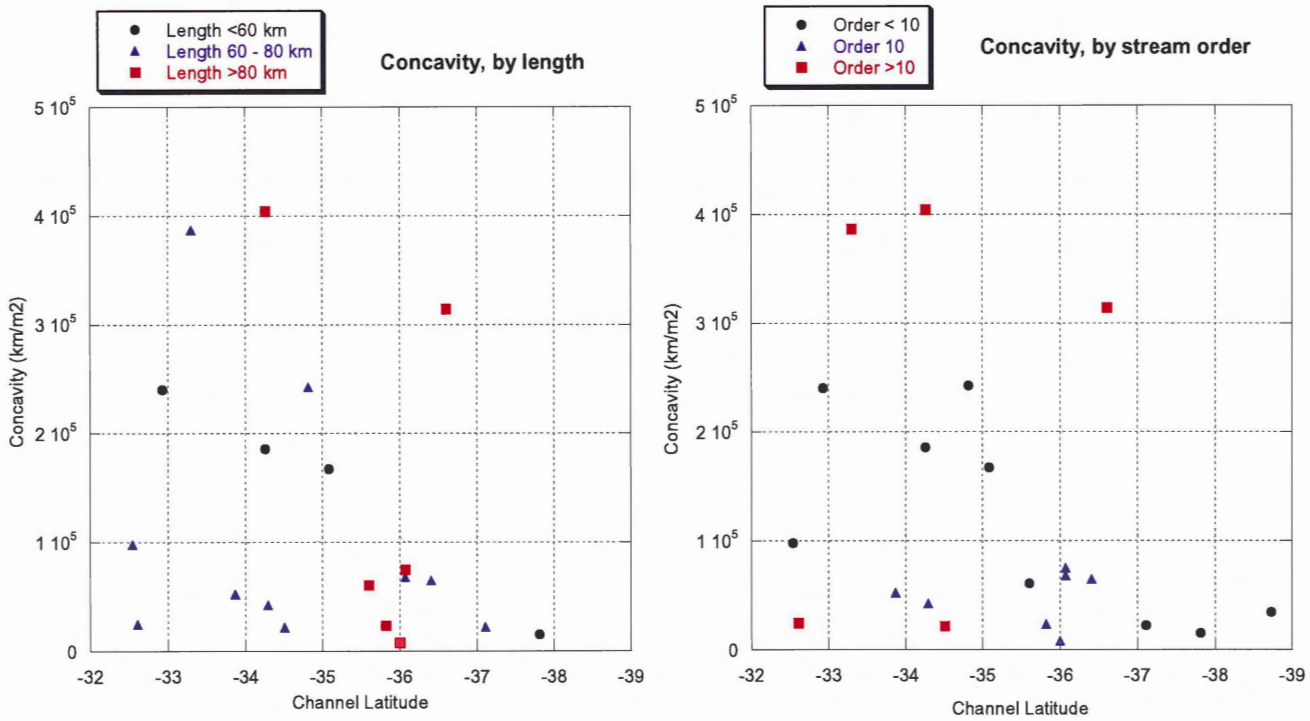

Figure 4.11 Concavity of all streams using method 2 (a) with streams sorted by length, and (b) with streams sorted by stream order.

4.4 Hypsometry

Hypsometry is the measurement and analysis of the distribution of land area lying at different elevations (Keller and Pinter 2002). It is possible to analyze the relationship between elevation and the area which lies *above* it (Strahler 1952), but it also possible to analyze the area which lies *below* the given elevation (Brocklehurst 2002). Eleven basins were used in this analysis- they extend from the drainage divide to the mountain front. The size and relief of the basin are independent of hypsometric shape (Keller and Pinter 2002) hence basins of various sizes were permitted for comparison. The integrals of these curves show a decreasing trend and the slope of the hypsometric curve at the point of inflection shows a very strong decreasing trend. Hypsometric integrals must be used with care when comparing basins because the integral is not unique to a single hypsometric shape.

Sigmoidal curves were used to approximate the shape and to determine the hypsometric integral and slope. This allowed the curve to be represented by a unique equation, which simplified these calculations. A program available online provided a simple conversion of the river curves derived from RiverTools into sigmoidal approximations. ZunZun.com is an interactive 2-dimensional and 3-dimensional data modeling which provides quality curve fitting and surface fitting.

Twenty three basins were initially chosen for hypsometric analysis however only 11 were used in this analysis. The remaining 12 basins had unresolved artifacts in their DEM data (missing data, boundary effects) that significantly affected the hypsometric analysis.

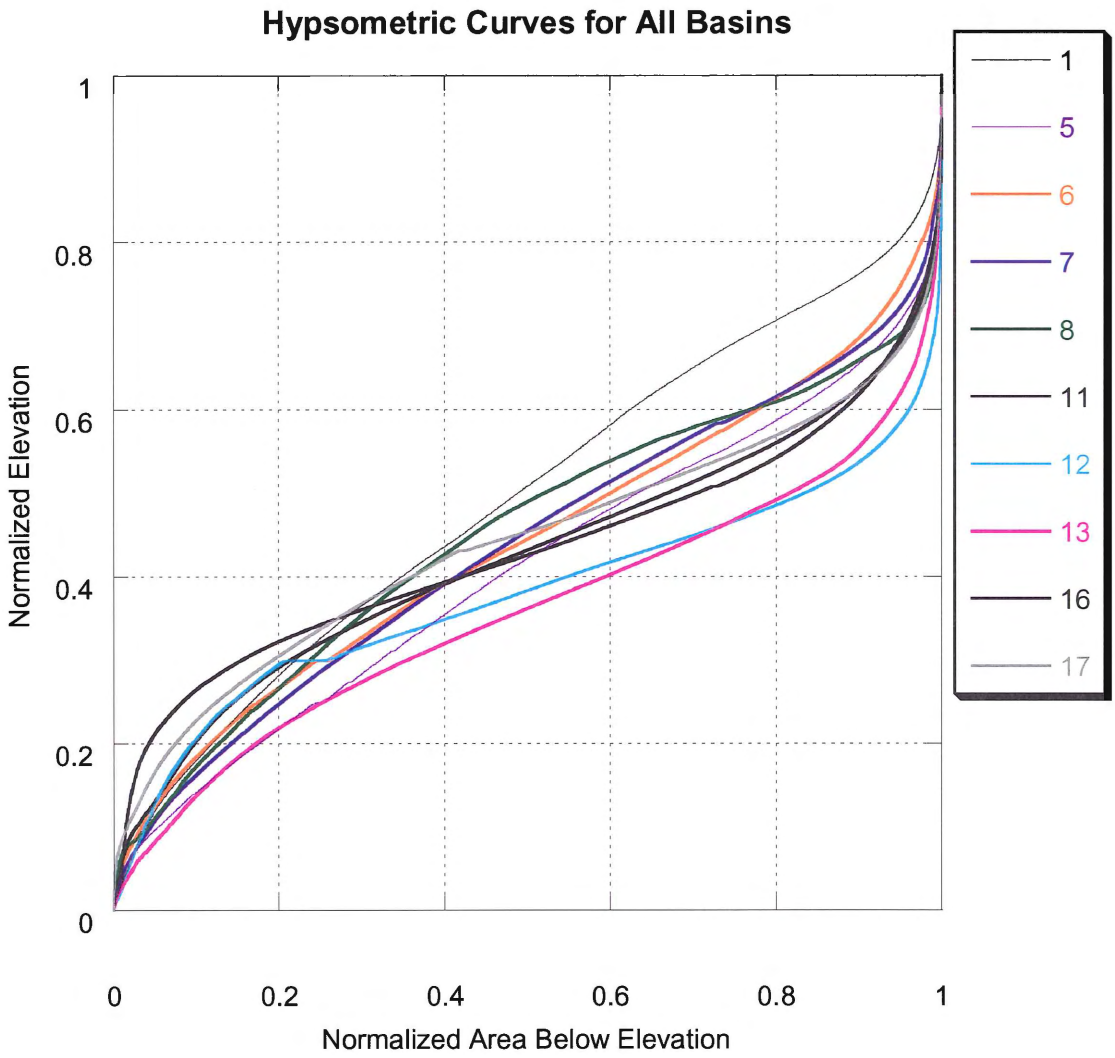

Figure 4.12 Hypsometry of all basins defined in figure 4.5. Hypsometries show the proportion of the area of a basin which lies beneath a given elevation and these are used to associate basins of similar maturity.

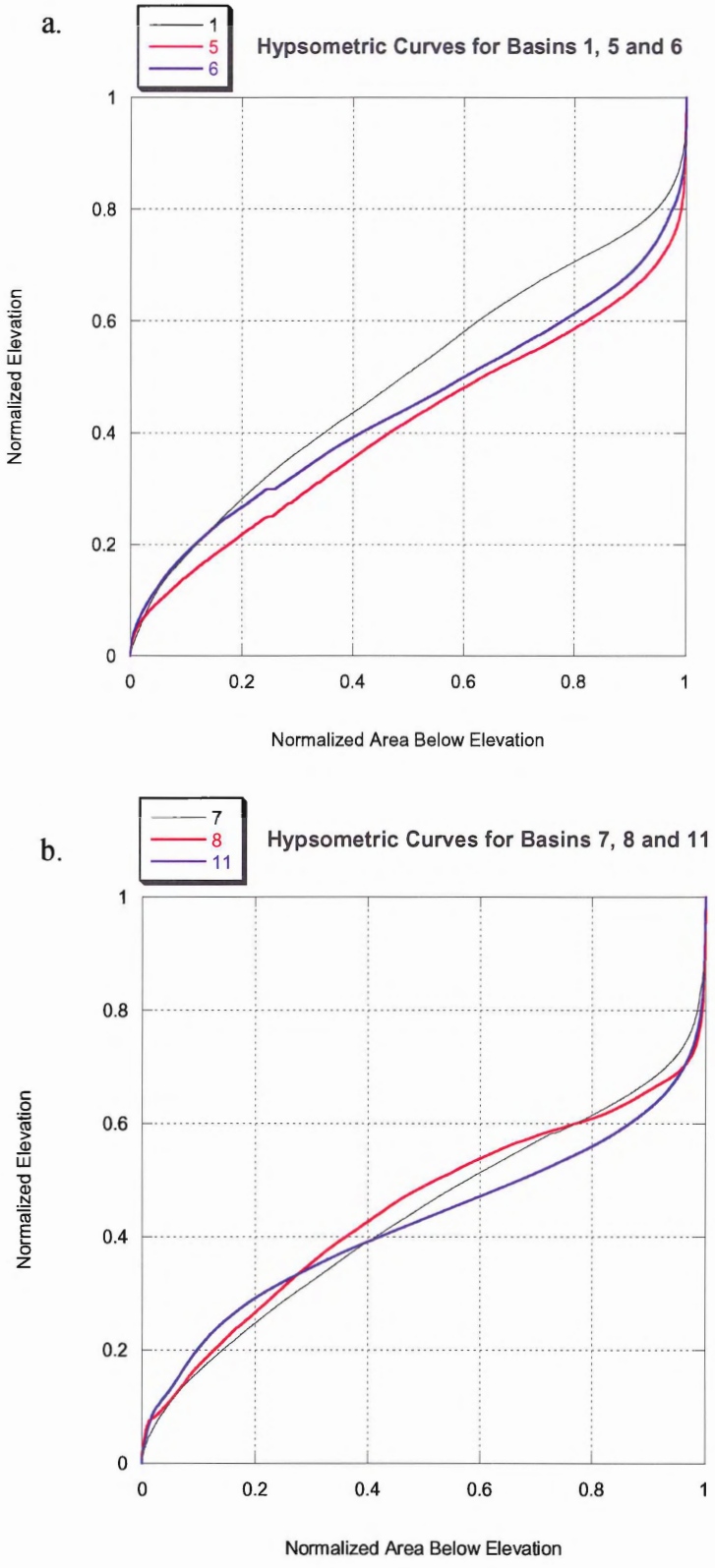

Figure 4.13 (a) and (b) Hypsometry of basins in the north and central region of the study area.

c.

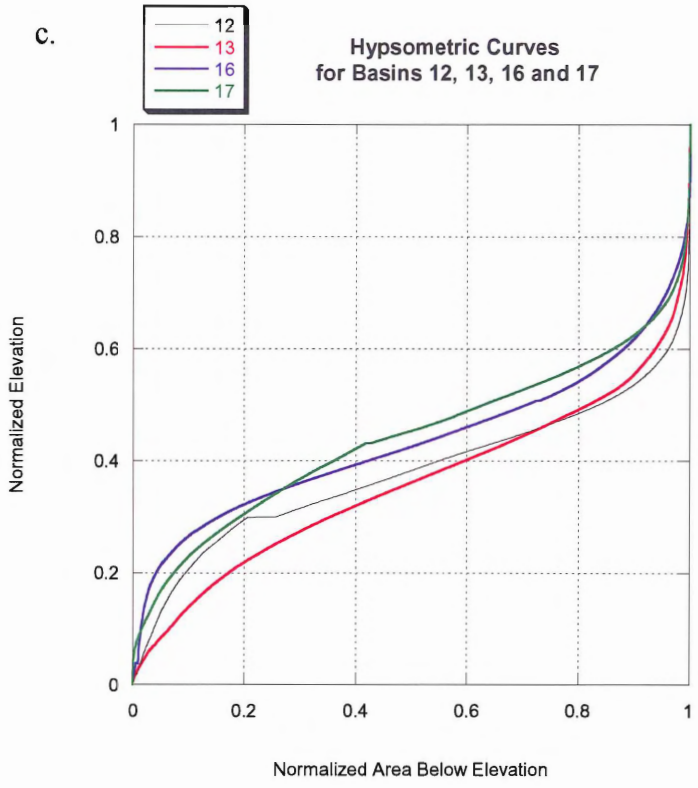

Figure 4.13 (c) Hypsometry of basins in the central region of the study area.

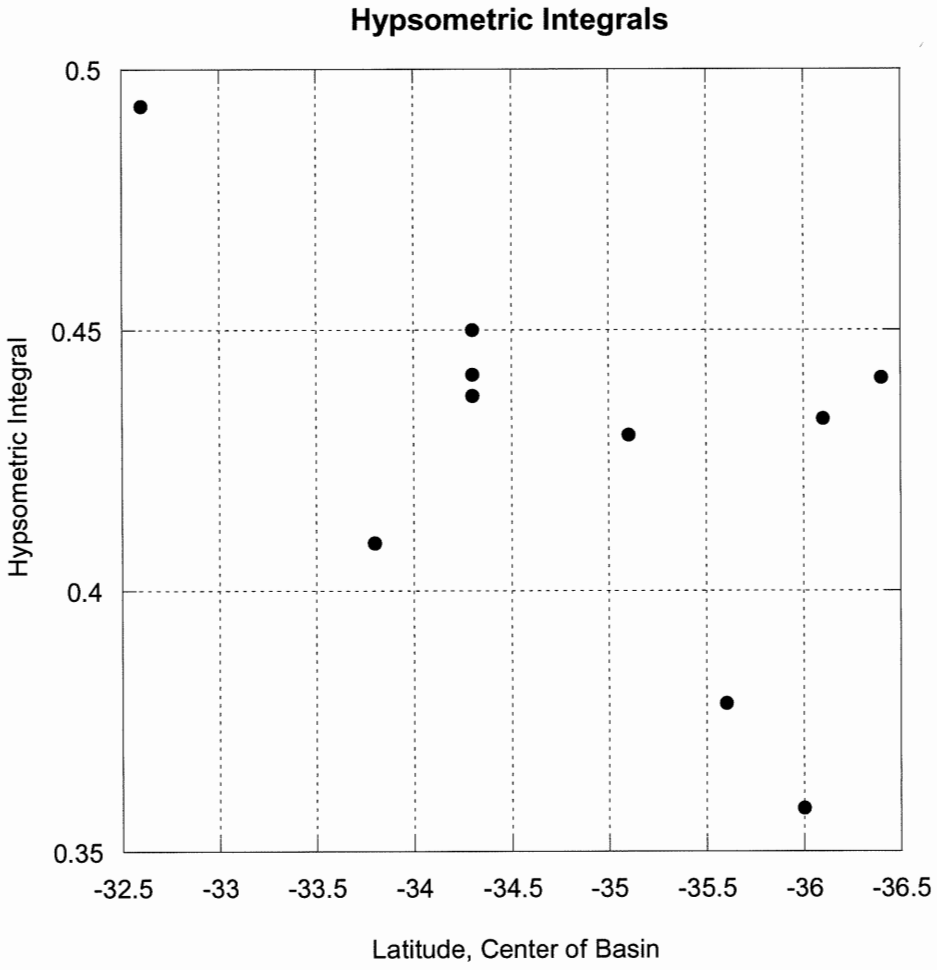

Figure 4.14 Hypsometric integrals of all basins. The hypsometric integrals show the area beneath the hypsometric curve of a basin and these can be used to associate basins of similar maturity. There is a trend toward decreasing hypsometric integrals from north to south.

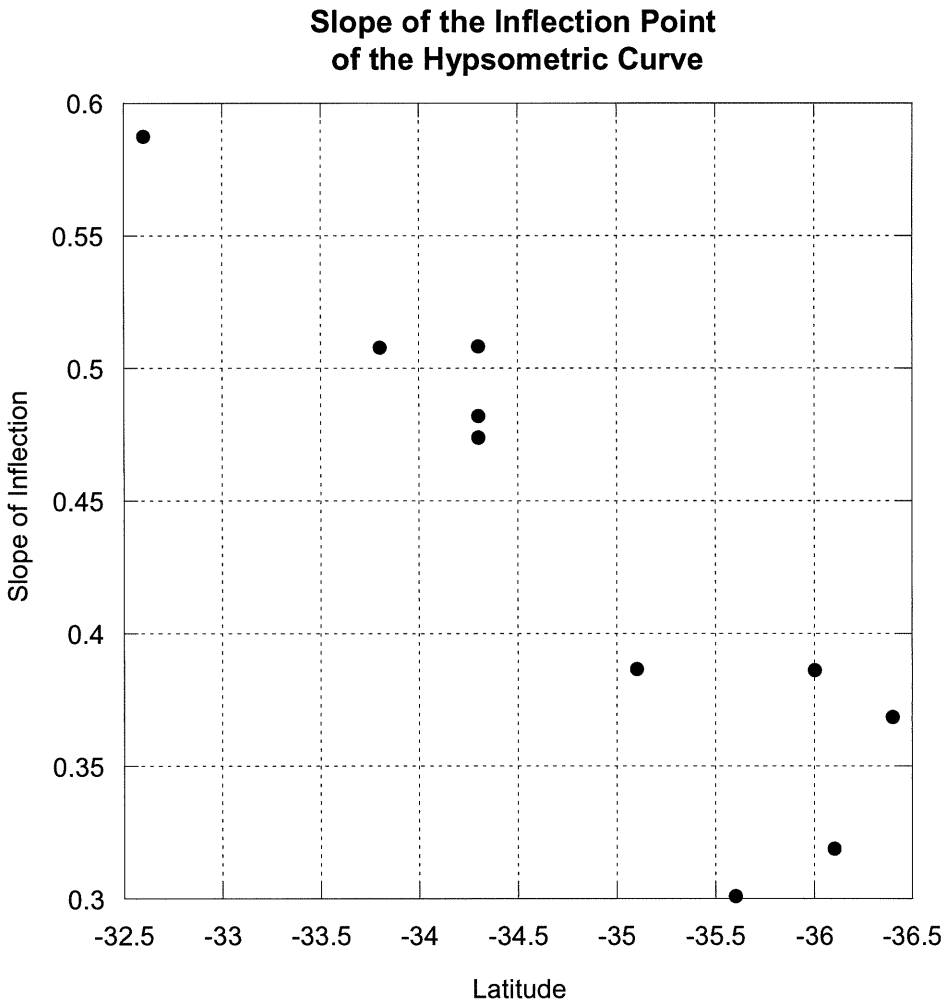

Figure 4.15 The slope of the inflection point of all basins. The inflection point in a hypsometric curve is used to associate basins of similar shapes. There is a strong trend toward decreasing slope of inflection point from north to south.

4.5 Tributary Symmetry

Tributary asymmetry uses the lengths of streams on either side of a major channel to describe changes in uplift on either side of the drainage basin (Fig. 3.7). This method has been shown to be an effective way to measure differential uplift (Cox 1994, Keller and Pinter 2002). In this analysis, streams which run east to west show a trend of longer streams in the north. This equates to uplift in the north for these streams. Analysis of tributary lengths revealed some patterns of uplift (or tilt) in the study area. This test considers the effect of tilting a landscape on the tributaries of a river system- where the land is tilted upwards streams will be longer (Fig. 3.6), and where land is tilted downward streams will be shorter (Keller and Pinter 2002). In streams trending east-west, long streams in the north indicated that upward tilt was predominantly in the north. This trend changes between 35° and 36°, where there are no east-west trending streams, and in the south there does not appear to be any clear uplift pattern.

In streams trending north-south, the trend is clearer in the south. Streams in this area show long tributaries in the west indicating upward tilt was in the west, whereas in the north streams exhibit little to no uplift.

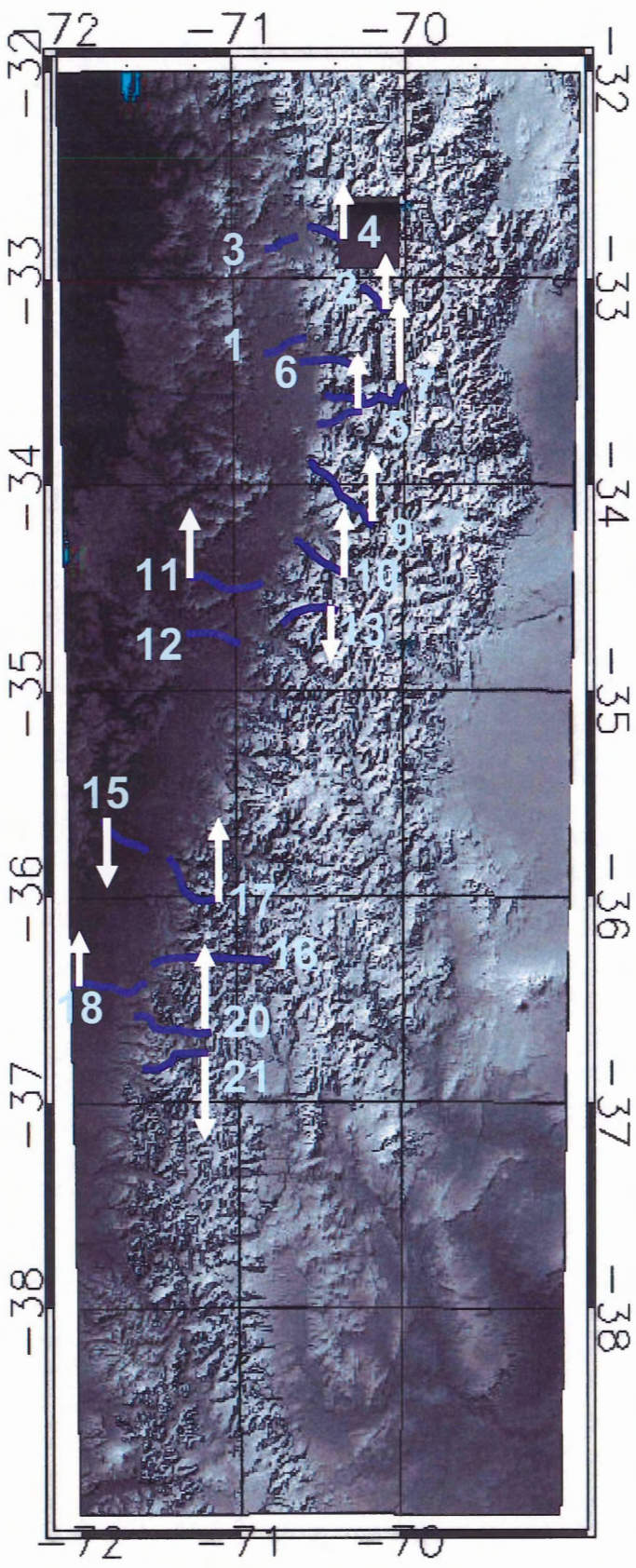

Figure 4.16 Location map of east-west trending streams and the proportional upward tilting of the drainage basins of these streams. North-south uplift trends determined from east-west tributary asymmetry shows upward tilting in the north. Arrows represent proportional upward tilting using figure 4.17.

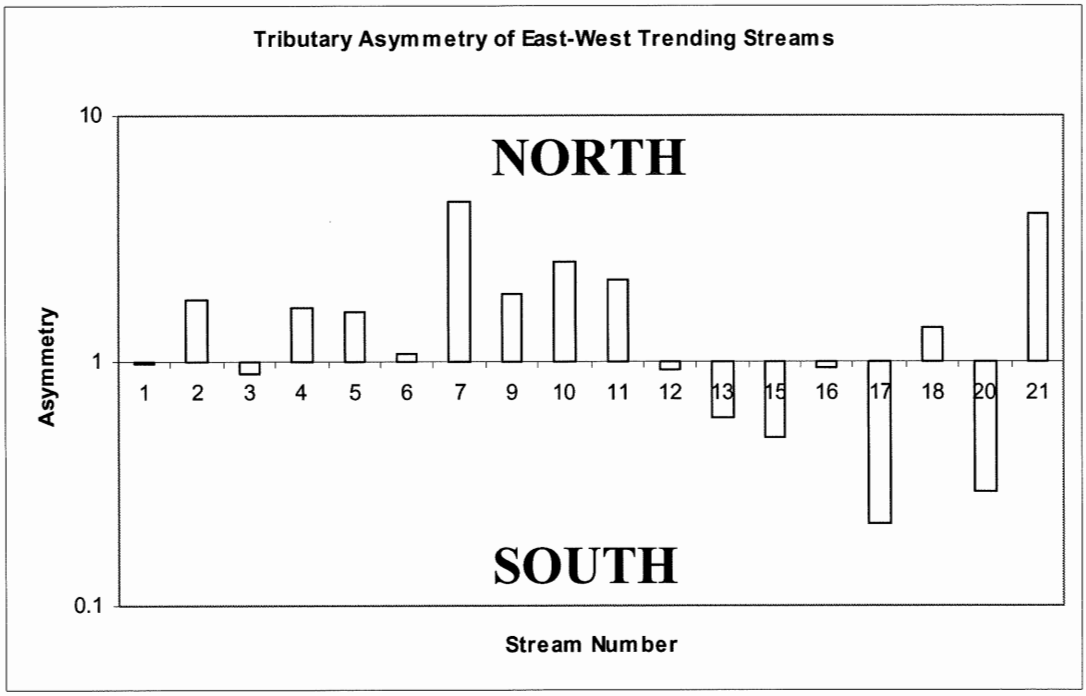

Figure 4.17 Tributary asymmetry results for east-west trending streams. Bars represent the ratio of the sum of the lengths of streams north of the main channel to the lengths of streams south of the main channel (asymmetry = Σ north streams/ Σ south streams). The scale for asymmetry is shown in the logarithmic scale in order to show the change relative to a symmetry of 1.

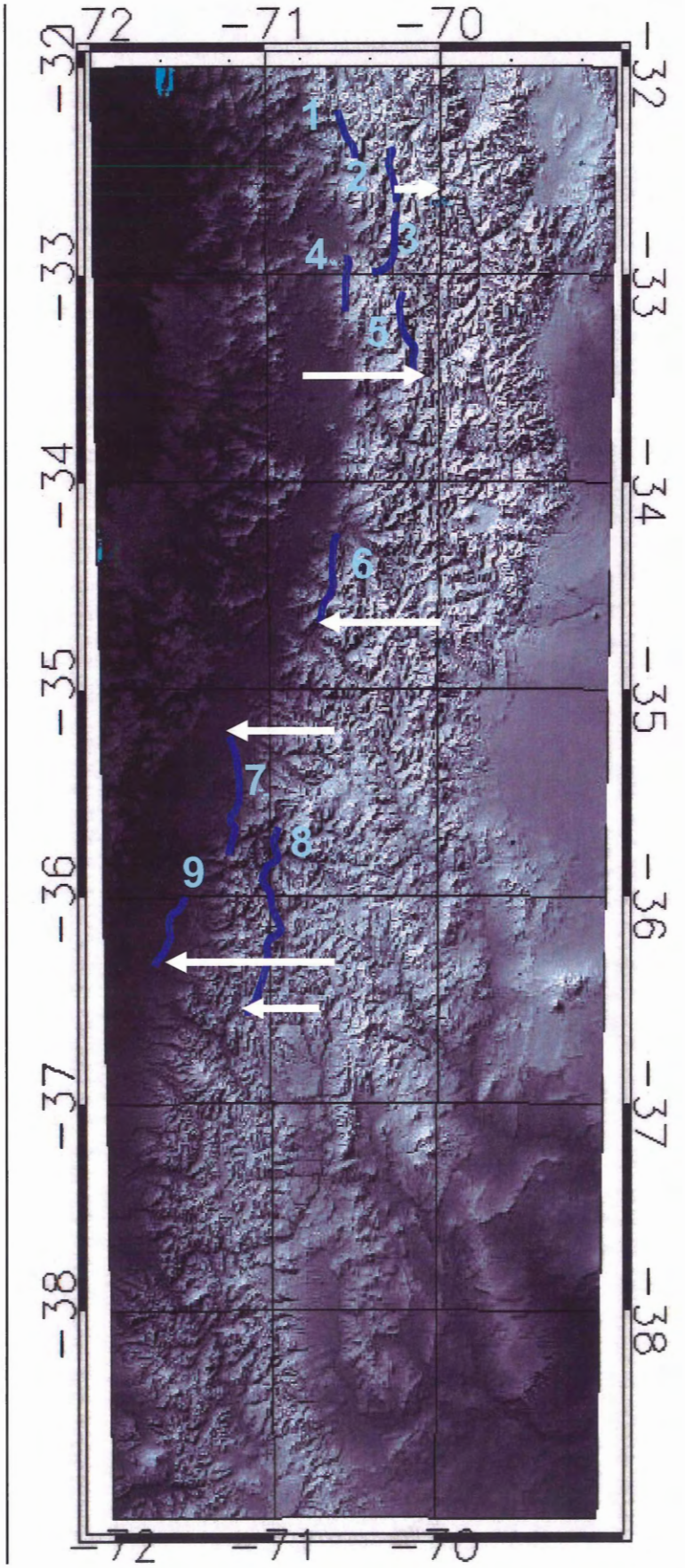

Figure 4.18 Location map of north-south trending streams and the proportional upward tilting of the drainage basins of these streams. East-west uplift trends determined from north-south uplift trends in the south of the study area show upward tilting in the west. Arrows represent proportional upward tilting values from figure 4.19.

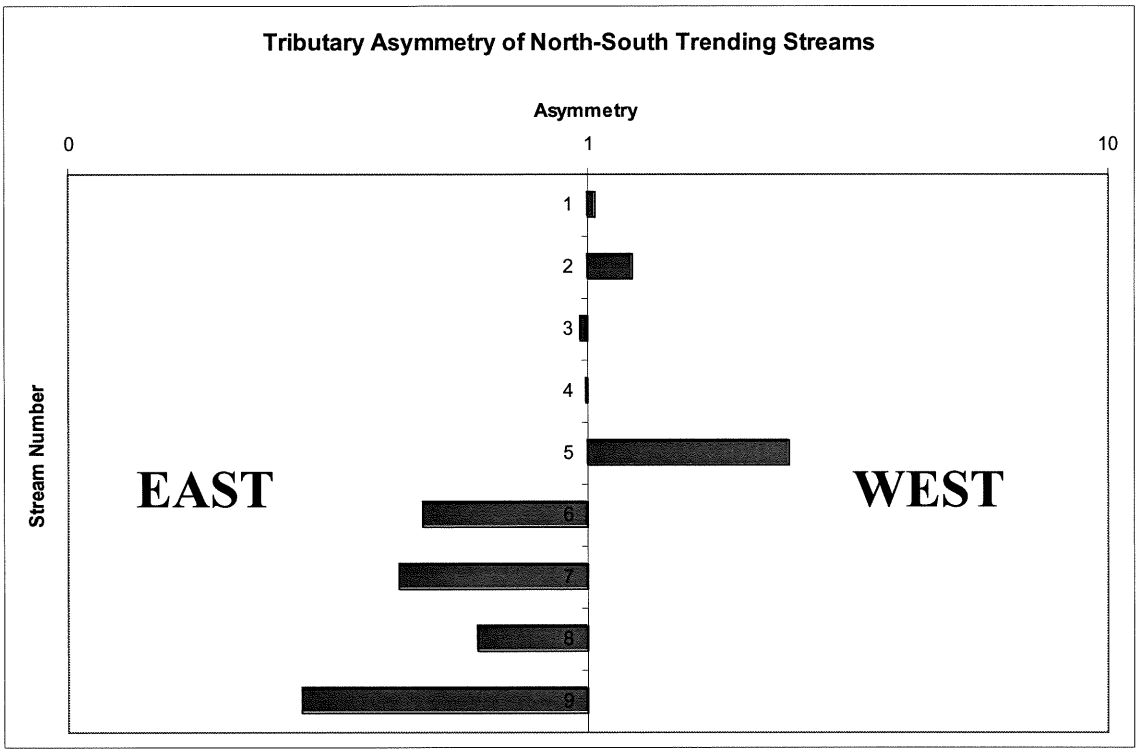

Figure 4.19 Tributary asymmetry results of north-south trending streams. Bars represent the ratio of the sum of the lengths of the streams east of the main channel to the lengths of the streams west of the main channel (asymmetry = Σ east streams/ Σ south streams). The scale for asymmetry is shown in the logarithmic scale in order to show the change relative to a symmetry of 1.

4.6 Mountain Front Sinuosity

The sinuosity of a mountain front describes the relative influence of tectonic forces (sinuosity ~1) and erosional forces (sinuosity > 1). Mountain front sinuosity was measured using a 5 km resolution, on 50 km sections of the Andes between 32° and 39°S. Measurements were taken at the point along the base of the mountain front which showed the greatest increase in slope. This resolution allowed for accurate tracing measurements along the mountain front using a topographic analysis software package (ArcMap). Sinuosity shows a very slight increase moving south along the mountain front, but there is a high degree of variability in both the east and west mountain fronts.

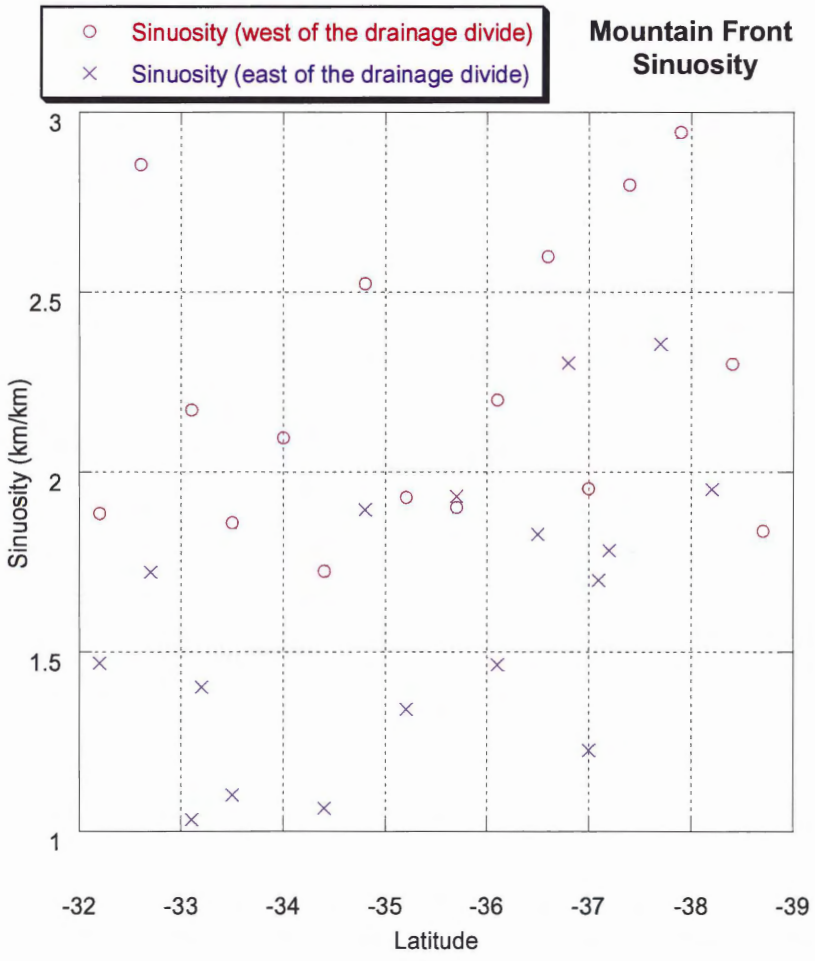

Figure 4.20 Sinuosity of the mountain front measured using a 5 km resolution along 50 km sections of the front from a 90m resolution DEM in ArcMap.

4.6 Area slope analysis

By plotting streams according to their slope and drainage area, it is possible to identify the dominant processes of incision for that basin (Sklar and Dietrich 1998). Basins chosen for hypsometric analysis were also appropriate for area slope analysis. Streams approaching a steady state will follow a predictable pattern of slopes and drainage area depending on their Strahler order and this pattern is evident in all basins in the study area. Lower order streams have high slopes and low drainage areas, and high order streams have high drainage areas and low slopes (Sklar and Dietrich 1998). It is significant that in the basins chosen for this analysis, streams of order greater than 4 consistently have drainage areas which are greater than 1 km^2. Figure 3.9 shows a basin excluded from the analysis because of its small drainage area. The graph shows streams of order 5 and 6 with drainage areas close to or less than 1 km^2.

Basins 1 and 5 (Fig. 4.21) showed very similar shapes in the frequencies of to each order above or below the transition zone between debris flow mechanics and bedrock-fluvial erosion mechanics. Basin 1 and 8 also have very similar distributions, but basin 8 shows a higher incidence of debris flow processes in the high order streams. Channels 5 and 7 show similar distribution patterns in the change of tributary slopes with increasing order, however the slopes in basin 7 are more constrained around a smaller range of slopes. Basins 11, 13, 16 and 17 show similar distribution patterns of channel slope and area. There is a relatively low range of upper slopes for all tributaries and highest order streams in these basins are purely affected by bedrock-fluvial processes. This analysis was limited by the minimum slopes and basin sizes which RiverTools could extract from the DEM, however these did not have a significant effect on the basins.

a.

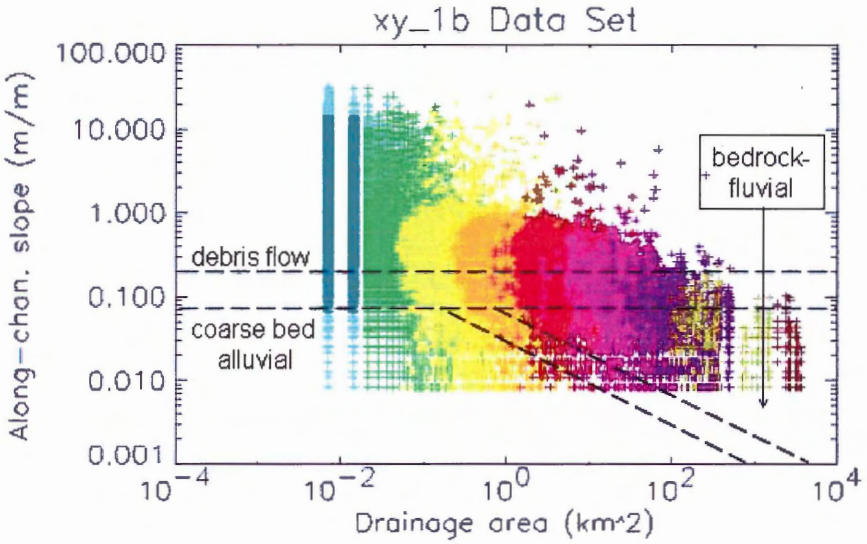

b.

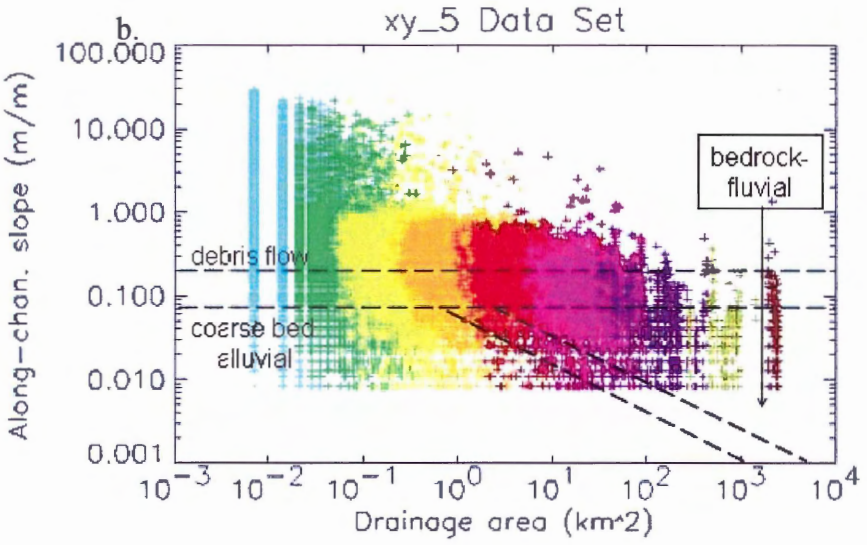

Figure 4.21 Analysis of basins plotting the drainage area of the reach against the along-channel slope of each reach in (a) and (b) basins 1 and 5.

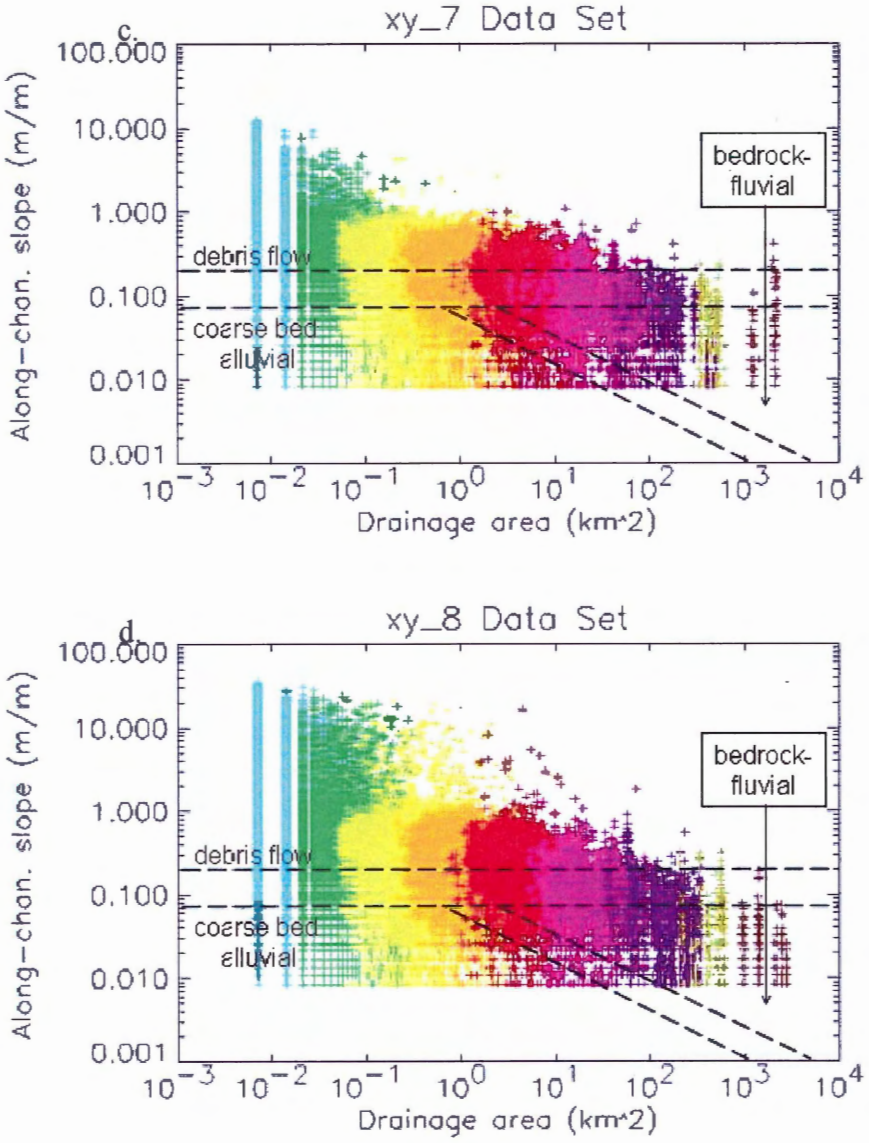

Figure 4.21 (c) and (d) Area-slope analysis of all streams in basins 7 and 8.

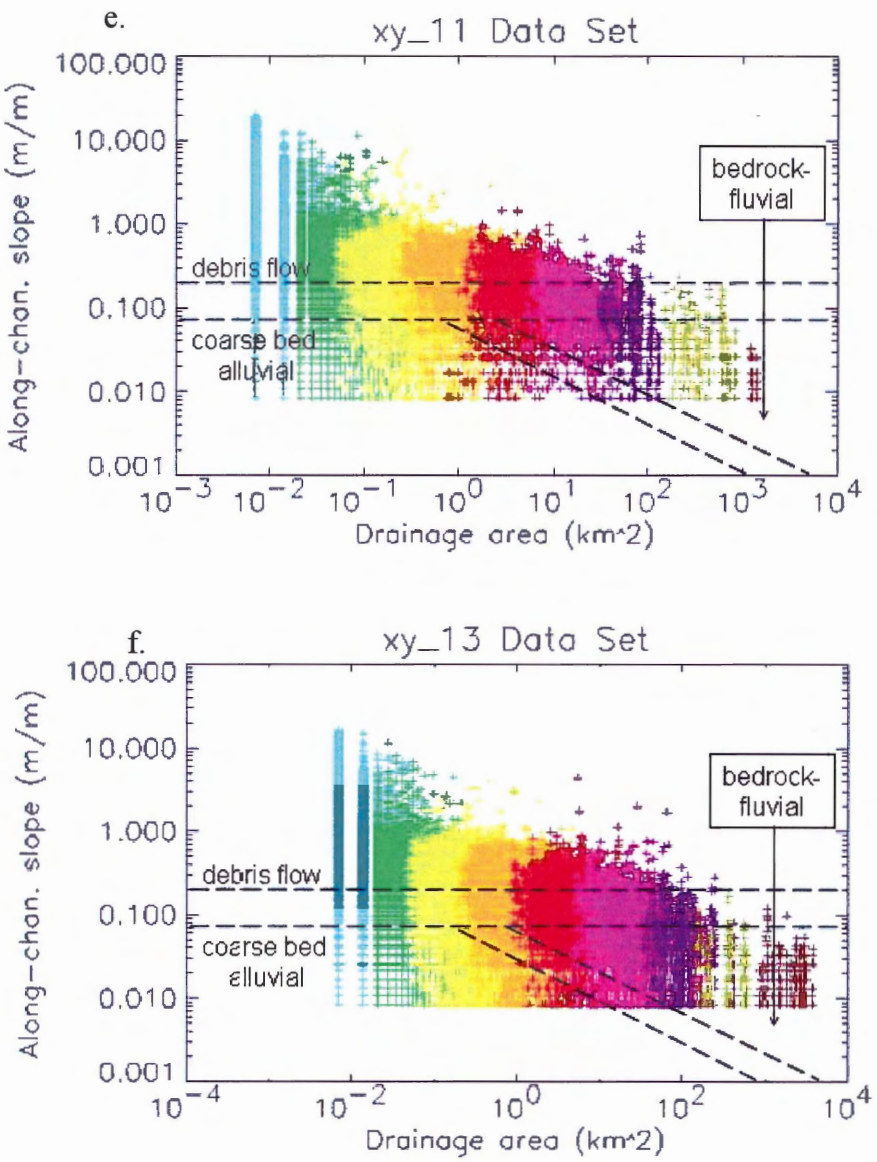

Figure 4.21 (e) and (f) Area-slope analysis of all streams in basins 11 and 13.

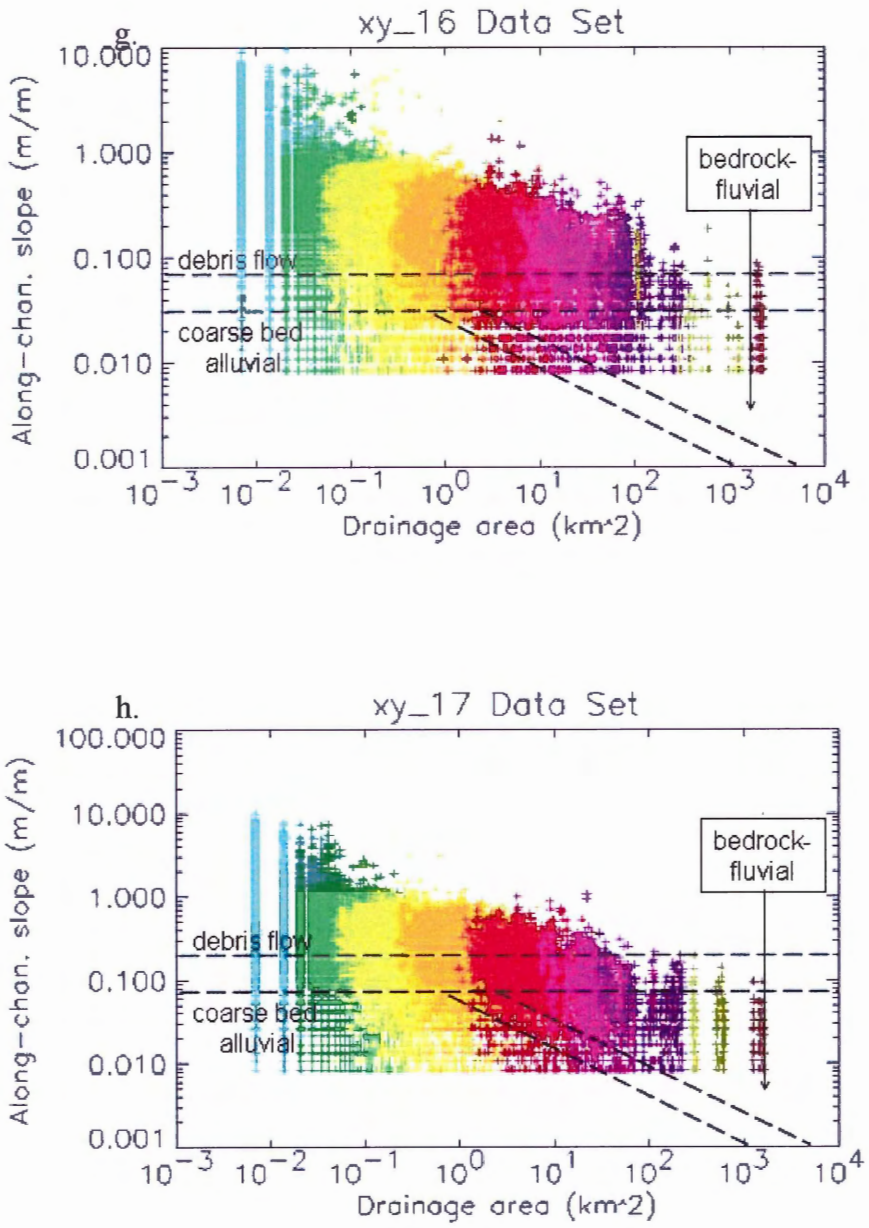

Figure 4.21 (g) and (h) Area-slope analysis of all streams in basins 16 and 17.

4.8 Synthesis of Results

The Andes between 32° and 39° show a change in elevation between 35° and 36°, from high elevation north of this zone to low elevation south of this zone. Using these three zones, the goal of this analysis was to determine if other geomorphometric indices existed which also distinguish these three zones. From 32° to 35°S, mean relief is 430.7 ± 108 m and from 36° to 39° mean relief is 189.2 ± 76.3 m. Basin relief ranged from 2.5 km to 4.8 km, with decreasing values toward the southern latitudes. Longitudinal profiles of streams showed the influence of lithology and faults on stream shape throughout the study area. There was no significant correlation between latitude and the concavity of these profiles. Hypsometric integrals show a weak decreasing trend, but the slope of the hypsometric curve at the point of inflection produces a very strong decreasing trend toward the south. Tributary asymmetry shows upward tilt in the northern latitudes and in the southern latitudes, upward tilting was to the west. Mountain front sinuosity is lowest in the north east of the drainage divide (sinuosity = 1.03), and highest in the south west of the drainage divide (2.35). Testing the study area using the area-slope relationship did not reveal a latitudinal trend however it did show that all streams of >5 strahler order have drainage area >10km^2.

Chapter 5.

Topographic analysis

5.1 Hypothesis rejected

The goal of this paper was to determine whether zones of topographic change could be defined in the Andes, between 32° and 39°S, using geomorphometrics and topographic characteristics determined from digital elevation maps. The hypothesis is rejected based on the results shown in table 5.1: Three zones are defined by changes in relief. From 32° to 35°, average relief is 430.7 ± 108 m, a narrow transition zone of decreasing relief exists from 35° to 36°, and from 36° to 39° mean relief is 189.2 ± 76 m. No other index could identify distinct zones of topographic change from 32° to 39°S. Basin relief showed a decreasing trend, as did the hypsometric integral of drainage basins. Mountain front sinuosity increased considerably from north to south. The slope of the hypsometric curve produced a very strong decreasing trend toward the south. Analysis of tributary asymmetry found active differential uplift in the region, with tilting in the north and in the south. The concavity of longitudinal stream profiles and the results of the area-slope analysis in the study area produced no convincing evidence of a latitudinal trend.

Parameter	Trend, from 32° to 39°
Relief	430.7 ± 108 m from 32° to 35° 189.2 ± 76 m from 36° to 39°
Basin Relief	Decreasing
Concavity	No Trend
Hypsometric Integral	Decreasing
Slope of hypsometric curve	Decreasing
East-west tributaries	Northward tilting in the north
North-south tributaries	Eastward tilting in the south
Mountain front sinuosity	Increasing
Drainage area-slope	No trend

Table 5.1 Summary of results. The results of geomorphic analysis using eight geomorphometric indices did not show three distinguishable zones in geomorphic indices expect for relief.

5.2 Major tectonic activity expressed

Figure 5.1 shows the major tectonic processes in the southern Andes. The Aconcagua fold and thrust belt lies between the drainage divide and the foreland basin of the Andes and comprises of 4 to 6 major, west-dipping thrust faults (Lavenu and Cembrano 1999, Giambiagi 2003, Allmendinger et al 1990). This belt has been active for more than 6 millions years and continues to be active today. The measurement of mountain front sinuosity was able to distinguish regions of high tectonic activity such as these. In the north, between 32° and 34°S east of the drainage divide, mountain front sinuosity determined this to be the region with the lowest sinuosity and hence the highest tectonic activity. This is the location of the north-south trending Aconcagua fold and thrust belt.

In more southern latitudes, the Chilean Lake District is located west of the continental divide and south of 36°S. This region is characterized by large basins, often filled by lakes, formed by extension along the fault zone (Kennan 2000) and also by the damning of glacial melt-water behind terminal moraines of retreating glaciers (Gosse, pers. comm.). The sinuosity of the mountain front in this region is high due to erosion by glacial scouring. Relatively low hypsometric integrals in basins from this region show glacial processes acting in this region. Tributary asymmetry showed upward tilting west of the continental divide at 36.6°S suggesting strong tectonic activity in this region. The active Liquine-Ofqui fault extends from 38° to 46° (Kennan 2000) and may influence uplift in this region (Lavenue and Cembrano 1999).

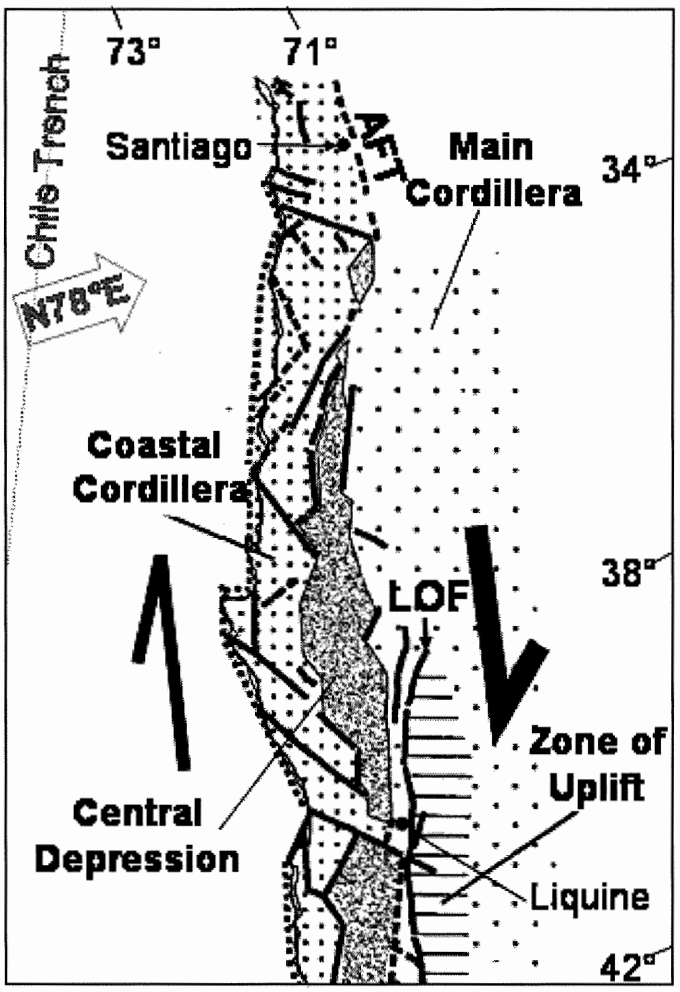

Figure 5.2 Simplified structural map of the southern Andes between 32° and 42°S. There is a strike-slip convergence between the Coastal and Principal (Main) Cordilleras, and the range is fragmented into several uplifted blocks. AFT = Aconcagua fold and thrust belt, LOF = Liquine-Ofqui Fault. Taken from Lavenu and Cembrano 1999.

A longitudinal valley extends from 32.5° to 34°S in the Mendoza Province (Fig. 3.10). These valleys lie east of the drainage divide and west of the fold and thrust belt.

In the north, the rivers drain into the Rio de los Palas, and in the south they drain into the Rio Tunuyan, and they are divided near Mount Tupingatito (Fig. 3.10). These valleys are similar to valleys found further north in the Eastern Cordillera of Bolivia (Kennan 2000). Paleodrainage is thought to have run north-south with drainage running east into foreland basin during the Late-Miocene (Kennan 2000). Tributaries show asymmetry in both north-south and east-west trending streams in this region. Upward tilting occurs in the east and in the north along streams in the longitudinal valley (Fig. 4.16, 4.18). This uplift is concurrent with mountain front sinuosity tests which show high tectonic activity east of the divide between 32° and 34°S. Longitudinal valleys in other parts of the Andes have been uplifted more than 2000 m over the past 10 Ma (Kennan 2000), and tributary asymmetry results support this information.

5.3 Significant changes in morphology along strike

The most evident change in morphology from this analysis is an abrupt decrease in the average relief along the range. Elevation changes gradually from north to south and defines three zones, but the transition between mean relief 430 ± 108 m north of 35°, and mean relief 189.2 ± 76 south of 36° does not mirror this gradual change (Fig. 4.2). One reason for this change in relief is that peaks cannot persist at high latitudes when the Andes intersect the perennial snowline at 35°S (Montgomery et al 2001). Another reason is that higher rates of glacial erosion in this region effectively limit the elevation of the mountains (Brozovic et al 1997). South of 35°, elevation and relief are lower in the eastern cordillera than in the western range. The snow line altitude is higher in the

Coastal Cordillera than in the Principal Cordillera (Satoh 1979). This has the effect of limiting peak height to a lower elevation in the Principal Cordillera (Fig. 4.1 h,i,j,l,m,n).

Decreasing basin relief supports the results determined by the latitudinal transect method. Drainage basin relief was substantially higher than relief determined using the latitudinal transect method however this is acceptable because basin area is much higher than the spatial window of relief analysis of the transect method. One anomaly in basin relief is at latitude 32.7°S west of the drainage divide. The location of the basin is isolated from other basins in the study and therefore may represent different active processes affecting that region. Basin 1 is in an area where tributaries of east-west and north-south trending streams are near-symmetrical. Judging from tributary symmetry patterns, differential uplift west of the drainage divide in this region seems to be low and this is supported by increased mountain front sinuosity. These factors suggest the basin is mature or near-equilibrium, with a sinuous mountain front and decreased tectonic activity. Hypsometric analysis shows the basin has a high integral and slope of inflection point symptomatic of a basin which is *not* in equilibrium (Strahler 1952). This is an example of local circumstances affecting the shape of the hypsometric curve (Fig. 4.13) and integral (Brocklehurst and Whipple 2002).

5.4 Other latitudinal trends and correlations

At 36°S, basins 12 and 13 show relatively low hypsometric integrals (0.3785 and 0.3584 respectively) and slopes of the inflection point of the hypsometric curve (0.3012 and 0.3863). The hypsometric integrals suggest that these basins have lower relief, gentler slopes and gentler stream gradients (Strahler 1952) and that their surface has

experienced more glacial activity (Brocklehurst and Whipple 2002). These basins are no longer expanding in area and are approaching equilibrium stage (Strahler 1952). South of 35°, higher rates of erosion in glacial and periglacial environments preferentially incise the land at high elevations resulting in excess elevation at the glacial limit (Kennan 2000).

Concavity was measured using two methods which produced noticeably different latitudinal patterns. Using method 1, the highest concavity was found at 35°S, but using method 2 there is no such latitudinal trend. Concavity is related to the maturity and stability of a stream profile, and a high concavity infers that these streams are at or near equilibrium relative to other streams in the area. At these latitudes, there is substantial transition in differential uplift patterns as well as relief, and this suggests processes affecting stream profiles are active. This inconsistency, combined with the varying results in concavity using two different methods, suggests that there is no correlation between latitude and stream concavity.

Chapter 6.

Conclusions

Surficial and tectonic processes work together to produce many range scale features in a mountain chain such as the Andes. It has been well documented that the change in width of the range and volcanic activity in the southern Andes is related to the geometry of the subducting plate (Jordan et al 1983, Kennan 1999, Ramos et al 1996), but surficial processes also have substantial effect on the topography (Montgomery et al 2001, Markgraf 1987, Lamb 2003). It is also well known that the elevation changes from 35°S to 36°S from high peaks (6000 m) to low peaks (3000 m). The goal of this thesis was to determine whether there were quantifiable changes in other geomorphics parameters which defined three zones. Using relief, hypsometry, concavity, tributary asymmetry, mountain front sinuosity and area-slope analysis, it was not possible to define distinct zones of landscape change.

In the north, mean relief is 430.7 ± 108 m, and in the south, mean relief is 189.2 ± 76 m. Basin relief shows a decrease from 2.5 km in the northern latitudes to 4.8 km in the south. Tributary asymmetry reveals north-tilting uplift from 32° to 35° and east-tilting uplift from 37° to 39°S. Hypsometric integrals and the slopes of the hypsometric curves decrease from north to south in the basins selected for the study.

Using mountain front sinuosity and tributary asymmetry it was possible to distinguish the two zones of high tectonic activity in the study area: the areas surrounding the Aconcagua fold and thrust belt in the north and the Liquine-Ofqui fault in the south. The zone of increased tectonism in the Mendoza Province which

corresponds to the position of the Aconcagua fold and thrust belt also corresponds to an antecendant stream which has been uplifted more than 2000 m since the Late Miocene (Kennan 1999). The longitudinal valley located between 32° and 34°S was determined to represent paelodrainage flow similar to antecedent streams found further north in the Andes (Kennan 2000). The intersection of the Andes with the perennial snow line results in a decrease in the relief of the mountains at 35°S (Montgomery et al. 2001) . The difference in peak heights in the Coastal and Principal Cordilleras has the effect of limiting the Principal Cordillera to lower elevation peaks than those of the Coastal Cordillera.

Future work would in the fields of equilibrium line altitude, thermochronology and tectonics would greatly improve the understanding of the relationship between tectonic and surficial processes in the Andes between 32° and 39°. Thermochronology information for the southern Andes could determine relative ages and rates of uplift and erosion rates in the study area. A better understanding of slab-dip geometry of the subducting Nazca plate from 32° to 39° would also considerably improve our understanding of the relationship between tectonic and surficial processes.

References

Abele, G. 1989. The interdependence of Elevation, Relief, and Climate on the Western Slope of the Central Andes. Z. Geol. Paleont. Tiel. 1127-1139.

Allmendinger, R.W., Figueroa, D., Snyder, D., Beer, J., Mpodozis, C., and Isacks, B.L. 1990. Foreland shortening and crustal balancing in the Andes at 30°S latitude. Tectonics. **9**. 789-809.

Allmendinger, R.W., Ramos, V.A., Jordan, T.E., Palma, M., and Isacks, B.L. 1983. Paleogeography and Andean structural geometry, northwest Argentina. Tectonics. **2**. 1-16.

Anderson, R.S. 1994. Evolution of the Santa Cruz Mountains, California, through tectonic growth and geomorphic decay. Journal of Geophysical Research. **99**. 20161-20179.

Brocklehurst, S. and Whipple, K. 2002. Glacial erosion and relief production in the Eastern Sierra Nevada, California. Geomorphology. **42**. 1-24.

Brozovoc, N., Burbank, D., and Meigs, A. Climatic limits on landscape development in the northwestern Himalaya. Science. **276**. 571-574.

Burbank, D.W., and Anderson, R.S. 2001. *Tectonic Geomorphology*. Blackwell Science.

Burbank, D.W., and Pinter, N. 1999. Landscape evolution: the interactions of tectonics and surface processes. Basin Research. **11**. 1-6.

Cox, T. 1994. Analysis of drainage-basin symmetry as a rapid technique to identify areas of possible Quaternary tilt-block tectonics: An example from the Mississippi Embayment. Geological Society of America Bulletin. **106**. 571-581.

Frankel, K., and Pazzaglia, F.J. (unpub) Mountain front landscape evolution.

Giambiagi, L.B., and Ramos, V.A. 2003. Cenozoic deformation and tectonic style of the Andes, between 33° and 34° south latitude. Tectonics. **22**.

Hartley, A. J. 2003. Andean uplift and climate change. Journal of the Geological Society. **160**. 7-10.

Hovius, N. 2000. Macroscopic process systems of mountain belt erosion. *In*: Summerfield, M.A. (ed.) *Geomorphology and Global Tectonics*. Wiley. Chichester, 167-199.

Introcaso, A., Pacino, M.C., and Fraga, H. 1992. Gravity, isostasy and Andean

crustal shortening between latitudes 30 and 35°S. Tectonophysics. **205**. 31-48.

Jordan, T.E., Isacks, B.L., Allmendinger, R.W., Brewer, J.A., Ramos, V.A., and Ando, C.J. 1983. Andean tectonics related to geometry of subducted Nazca plate. Geological Society of America Bulletin. **94**. 341-361.

Keller, E.A., and Pinter, N. 2002. Active Tectonics: Earthquakes, Uplift and Landscape. Prentice-Hall Inc.

Kennan, L. 1999. Large-scale geomorphology of the Andes: interrelationships of tectonics, magmatism and climate. *In*: Summerfield, M.A. (ed.) *Geomorphology and Global Tectonics*. Wiley. Chichester, 167-199.

Kirkbride, M. and Matthews, D. 1997. The role of fluvial and glacial erosion in landscape evolution: the Ben Ohau Range, New Zealand. Earth Surface Processes and Landforms. **22**. 317-327.

Koi, H. and Beaumont, C. 1994. Escarpment evolution on high-elevation margins: Insights derived from a surface processes model that combines diffusion, advection, and reaction. Journal of Geophysical Research. **99**. 12191-12209.

Lamb, S., and Davis, P. 2003. Cenozoic climate change as a possible cause for the rise of the Andes. Nature. **425**. 792-797.

Lavenue, A. and Cembrano, J. 1999. Compressional- and transpressional-stress pattern for Pliocene and Quaternary brittle deformation in fore arc and intra-arc zones (Andes of Central and Southern Chile). Journal of Structural Geology. **21**. 1669-1691.

Liu, Z., and Bird, P. 2002. Finite element modelling of neotectonics in New Zealand. Journal of Geophysical Research. **107**.

Markgraf, V. 1987. Paleoclimates of the Southern Argentine Andes. Current Research in the Pleistocene. **4**. 150-157.

Montgomery, D.R., Balco, G., and Willett, S.D. 2001. Climate, tectonics, and the morphology of the Andes. Geological Society of America. **29**. 579-582.

Montgomery, D.R., and Brandon, M.T. 2002. Topographic controls on erosion rates in tectonically active mountain ranges. Earth and Planetary Science Letters. **201**. 481-489.

Pazzaglia, F. J., and Brandon, M.T. 2001. A fluvial record of long-term steady-state uplift and erosion across the Cascadia Forearc High, Western Washington State. American Journal of Science. **301**. 385-431.

Porter, S.C. 1975. Equilibrium-line altitudes of Late Quaternary glaciers in the Southern Alps, New Zealand. Quaternary Research. **5**. 27-47.

Radoane, M., Radoane, N., and Dumitriu, D. 2003. Geomorphological evolution of longitudinal profiles in the Carpathians. Geomorphology. **50**. 293-306.

Ramos, V.A., Cegarra, M., and Cristallini, E. 1996. Cenozoic tectonics of the High Andes of west-central Argentina (30-36°S latitude). Tectonophysics. **259**. 185-200.

Riquelme, R., Martinod, J., Herail, G., Darrozes, J., and Charrier, J. 2003. A geomorphological approach to determining the Neogene to Recent deformation of the Coastal Cordillera of northern Chile (Atacama). Tectonophysics. **361**. 255-275.

Satoh, H. 1979. On the snow-line altitude in the central and southern Andes of the modern age and the diluvial epoch. In S. Horie (ed.), Paleolimnology of Lake Biwa and the Japanese Pleistocene, 387-415.

Strahler, A. 1952. Hypsometric (area-altitude) analysis of erosional topography. Bulletin of the Geological Society of America. **63**. 1117-1142.

Tinkler, K and Wohl, E. 2002. Rivers Over Rock: Fluvial processes in bedrock

channels.American Geophysical Union.

Watts, A.B., McKerrow, W.S., and Fielding, E. 2000. Lithospheric flexure, uplift, and landscape evolution in south-central England. Journal of the Geological Society, London. **157**. 1169-1177.

Willemin, J.H., and Knuepfer, P.L.K. 1994. Kinematics of arc-continent collision in the eastern Central Range of Taiwan inferred from geomorphic analysis. Journal of Geophysical Research. **99**. 20267-20280.

Zaprowski, B.J., Pazzaglia, F.J., and Evenson, E.B. (unpub.) Climatic influences on longitudinal profile concavity.

Appendix

Latitude	Maximum elevation area (m^2)	Minimum elevation area (m^2)	Relief Area (m^2)	Total distance (km)	Relief (m)
32.1	654947.80	564836.40	90111.40	202.80	**444.35**
32.2	610993.10	540636.90	70356.20	212.84	**330.56**
32.3	584688.70	540891.50	43797.20	195.07	**224.53**
32.4	580023.60	505882.70	74140.90	203.46	**364.41**
32.5	622747.20	523527.80	99219.40	216.98	**457.28**
32.6	686881.60	629298.00	57583.60	251.30	**229.15**
32.7	590874.90	462283.60	128591.30	219.67	**585.38**
32.8	488387.70	371032.60	117355.10	208.29	**563.43**
32.9	552728.10	413974.00	138754.10	201.99	**686.93**
33.0	572818.90	483184.30	89634.60	209.07	**428.72**
33.1	540850.50	439819.50	101031.00	184.22	**548.43**
33.2	523347.80	419276.10	104071.70	174.31	**597.04**
33.3	446639.00	358832.30	87806.70	172.96	**507.68**
33.4	423833.00	348022.90	75810.10	171.91	**440.98**
33.5	463170.50	370900.50	92270.00	194.81	**473.64**
33.6	390521.80	301250.70	89271.10	186.71	**478.13**
33.7	370630.90	303321.90	67309.00	178.00	**378.14**
33.8	308983.30	270640.90	38342.40	132.54	**289.29**
33.9	509759.00	406069.40	103689.60	255.31	**406.14**
34.0	505704.60	384298.30	121406.30	237.28	**511.66**
34.1	512528.20	435570.30	76957.90	215.26	**357.51**
34.2	453739.80	369785.40	83954.40	240.68	**348.82**
34.3	397760.40	324988.90	72771.50	212.16	**343.00**
34.4	352351.30	277280.50	75070.80	203.87	**368.23**
34.5	438150.20	339976.70	98173.50	222.40	**441.43**
34.6	518923.40	428028.90	90894.50	239.14	**380.09**
34.7	591226.50	468976.90	122249.60	299.24	**408.53**
34.8	417461.00	317762.30	99698.70	213.67	**466.60**
34.9	373693.70	317472.10	56221.60	238.64	**235.59**

Table 1 (a) Determination of relief for latitudinal elevation plots, from 32° to 34.9°S. For each swath, a maximum and minimum elevation curve was determined. The area under each curve represents the integral and the total relief for the curve. Relief was calculated using the integral of the difference between the maximum and minimum curves, and factoring by the length of the swath.

35.0	519279.20	427909.30	91369.90	314.41	**290.61**
35.1	523377.20	492355.50	31021.70	312.41	**99.30**
35.2	524237.70	461035.40	63202.30	340.02	**185.88**
35.3	573607.30	486199.20	87408.10	350.65	**249.28**
35.4	346991.10	295290.90	51700.20	228.03	**226.73**
35.5	593684.60	551361.90	42322.70	342.09	**123.72**
35.6	622130.00	564888.80	57241.20	368.70	**155.25**
35.7	563165.90	507609.10	55556.80	354.67	**156.64**
35.8	480935.10	407233.70	73701.40	328.87	**224.11**
35.9	435955.90	338770.80	97185.10	267.29	**363.60**
36.0	573298.40	500797.80	72500.60	343.65	**210.97**
36.1	500989.50	486878.40	14111.10	347.36	**40.62**
36.2	548618.70	488349.00	60269.70	336.74	**178.98**
36.3	350809.80	284834.30	65975.50	161.55	**408.39**
36.4	556900.40	491401.70	65498.70	326.58	**200.56**
36.5	375167.60	339296.40	35871.20	252.08	**142.30**
36.6	437956.00	367667.60	70288.40	282.83	**248.52**
36.7	361960.60	301064.70	60895.90	262.99	**231.55**
36.8	420734.00	369945.90	50788.10	309.54	**164.08**
36.9	462374.60	410775.80	51598.80	349.60	**147.60**
37.0	385720.80	352342.10	33378.70	304.01	**109.80**
37.1	475853.30	387303.20	88550.10	357.91	**247.41**
37.2	417193.80	385923.10	31270.70	344.73	**90.71**
37.3	368867.50	323597.10	45270.40	369.69	**122.45**
37.4	480195.40	345303.90	134891.50	399.84	**337.37**
37.5	376651.90	311773.70	64878.20	332.33	**195.22**
37.6	340805.30	286649.20	54156.10	312.86	**173.10**
37.7	350853.20	286411.10	64442.10	330.53	**194.97**
37.8	417233.30	355385.20	61848.10	376.90	**164.10**
37.9	347954.20	289955.10	57999.10	308.24	**188.16**
38.0	305648.10	230963.80	74684.30	304.49	**245.28**
38.1	338877.60	263804.00	75073.60	321.36	**233.61**
38.2	294233.10	242111.20	52121.90	251.36	**207.36**
38.3	243686.80	207378.30	36308.50	268.62	**135.17**
38.4	267180.10	237994.90	29185.20	286.70	**101.80**
38.5	248371.70	175184.00	73187.70	235.90	**310.26**
38.6	291447.90	242407.80	49040.10	296.19	**165.57**
38.7	335352.50	303424.40	31928.10	305.04	**104.67**
38.8	273452.40	227862.40	45590.00	200.23	**227.69**
38.9	187809.00	169491.00	18318.00	123.78	**147.99**

Table 1 (b) Determination of relief for latitudinal elevation plots, from 35° to 39°S. For each swath, a maximum and minimum elevation curve was determined. The area under each curve represents the integral and the total relief for the curve. Relief was calculated using the integral of the difference between the maximum and minimum curves, and factoring by the length of the swath.

Outlet Number	Outlet x-coordinate	Outlet y-coordinate	Outlet pixel ID	Outlet parent pixel ID	Outlet elevation (m)	Basin area (km^2)	Basin relief (km)	Pruning method:	Pruning threshold:
1	-70.6775	-32.553333	2388386	2391985	989	1015.2939	3.395	Order	3
2	-70.465	-32.855	3691841	3688240	1006	2105.9397	4.2	Order	3
3	-70.474167	-33.363333	5887830	5887829	896	649.33936	3.959	Order	3
4	-70.485	-33.595833	6892217	6892216	760	3334.7727	4.523	Order	3
5	-70.61	-34.266667	9790067	9790066	663	2727.1321	4.262	Order	3
6	-70.761667	-34.739167	11831085	11827484	652	1420.9568	3.682	Order	3
7	-70.870833	-34.985	12892954	12896553	590	1241.868	3.061	Order	3
8	-71.0025	-35.281667	14174396	14177995	643	1365.4298	3.078	Order	3
9	-71.173333	-35.724167	16085791	16085790	433	3214.187	3.404	Order	3
10	-70.956667	-36.000833	17281251	17277650	859	1874.8473	1.994	Order	3
11	-71.479167	-36.608333	19905024	19901424	483	1562.2522	2.631	Order	3
12	-71.708333	-37.319167	22975549	22975548	504	2331.4734	2.576	Order	3
13	-71.711667	-37.7725	24933945	24930344	336	1383.7383	2.499	Order	3
14	-71.511667	-38.000833	25920585	25916984	550	4739.5103	2.058	Order	3
15	-69.564167	-32.735	3174522	3174523	2054	3215.7498	4.383	Order	3
16	-69.386667	-33.865	8056335	8056336	1567	2291.1301	4.837	Order	3
17	-69.58	-34.586667	11173703	11177304	1803	2089.3545	3.223	Order	3
18	-69.6825	-34.970833	12833180	12829581	1751	874.08905	3.032	Order	3
19	-70.0025	-35.835833	16569596	16569597	1500	3825.0488	2.803	Order	3
20	-70.0025	-36.694167	20277596	20277597	1091	2263.1035	3.088	Order	3
21	-70.45	-37.345833	23092259	23088660	876	8283.5283	3.428	Order	3
22	-70.279167	-37.3475	23099664	23103264	859	2180.5227	2.908	Order	3
23	-70.471667	-38.494167	28053033	28053034	745	3155.0649	1.786	Order	3

Table 2 (a) Attributes of basins defined in figure 4.4 including coordinates define the location of the outlet, outlet elevation relative to sea level, basin area and relief, pruning method uses Strahler order with threshold of order 3.